Highly Stretchable, Transparent, and Adhesive Double Network Hydrogels for the Development of Wearable Strain Sensors

by

Xin Yi Dong

A thesis submitted in partial fulfillment of the requirements for the degree of

Master of Science

in

Chemical Engineering

Department of Chemical and Materials Engineering
University of Alberta

© Xin Yi Dong, 2024

Abstract

The exploration of high-performance hydrogels in this thesis marks the convergence of biomedical engineering and wearable technology. This study delves into the creation and use of a novel silicotungstic acid (SiW)-based hydrogel, designed specifically for wearable strain sensors. Mimicking human tissue mechanics, the SiW hydrogel emerges as an ideal candidate for wearable medical devices.

Recent strides in wearable medical technology, notably spurred by the healthcare challenges of the COVID-19 pandemic, have highlighted the urgent need for materials capable of constant, real-time physiological monitoring. Hydrogels, noted for their high water content and adaptability, have gained significant traction in a variety of biomedical and everyday uses. Yet, finding a hydrogel that perfectly balances mechanical strength, electrical conductivity, and biocompatibility remains a considerable challenge.

This research introduces a SiW-based hydrogel, crafted through a facile one-pot method. This process involves the radical polymerization of acrylamide (AM) with Methylenebisacrylamide (MBAA) and Carboxymethyl cellulose (CMC), resulting in a double-network hydrogel that excels in ionic conductivity and moisture retention. This makes it an ideal solution for wearable strain sensing. The study further investigates the hydrogel's impressive stretchability, adhesiveness, and transparency, and its potential application towards a wearable strain sensor.

Historically, research on SiW-based hydrogels has primarily focused on their adhesive properties, often at the expense of mechanical strength (cohesion). In this study, we present a novel approach to fabricate a polysaccharide hydrogel that harmoniously balances both adhesion and cohesion via interfacial hydrogen bonds. This hydrogel, composed of carboxymethyl

cellulose, PAM, silicotungstic acid, and LiCl, showcases a unique combination of properties: strain-responsive ionic conductivity, superior transparency, remarkable stretchability, and robust adhesion. Contrary to conventional PAM hydrogels, our PAM-SiW networked hydrogel addresses the common challenge of achieving good adhesion without compromising on cohesion. Specifically, our hydrogel demonstrates a maximum toughness of 20.3 MJ/m^3 and a strain of 4079%, a feat rarely observed in similar hydrogels. Furthermore, the hydrogel's adhesion is both reversible and versatile, adhering effectively to a variety of wet and dry substrates. This makes it a promising candidate for advanced healthcare applications, particularly as a mechanically reinforced underwater adhesive with unparalleled stability. We also provide insights into the role of LiCl in the hydrogel matrix, emphasizing its influence on electrostatic interactions without affecting the hydrogen bonds. This study serves as a testament to the potential of harmonizing adhesive and cohesive properties in hydrogels, paving the way for future innovations in the field.

The thesis comprehensively covers the formulation, analysis, and practical applications of the SiW hydrogel. It underscores the hydrogel’s ability to adapt to skin, endure environmental challenges, and remain functional under various conditions. The exploration of its adhesion properties, especially in different moisture conditions, signifies a substantial step forward in hydrogel technology.

Acknowledgement

At the culmination of this academic journey, I find myself reflecting on the invaluable contributions and unwavering support I have received. It is with profound gratitude that I acknowledge those who have played an instrumental role in the fruition of this thesis.

First and foremost, my sincerest thanks go to my thesis advisor, Dr. Hongbo Zeng, whose expertise, insightful guidance, and patient mentorship have been the cornerstone of this research. Your encouragement and rigorous academic standards have not only shaped this work but have also greatly contributed to my personal and professional growth.

I extend my heartfelt appreciation to the members of my thesis committee for their invaluable feedback, constructive criticism, and scholarly engagement throughout this process. Your perspectives and suggestions have immensely enriched this work.

A special note of thanks goes to my lab colleagues and peers, whose camaraderie, collaborative spirit, and intellectual exchanges have made my time in the laboratory both productive and enjoyable.

I am deeply grateful to the staff at the University of Alberta Department of Chemical and Materials Engineering, whose administrative support and guidance have been indispensable. Your efforts behind the scenes have facilitated a conducive research environment.

My heartfelt gratitude extends to my friends and family. Your unwavering belief in me, constant encouragement, and endless patience have been my strength. This accomplishment is as much yours as it is mine.

This journey has been both challenging and rewarding, and I am profoundly grateful for the support and guidance of each individual who has been a part of it. Thank you for contributing to my growth as a researcher and for being a part of my academic endeavor.

Table of Contents

Abstract ii
Acknowledgement iv
List of Tables vii
List of Figures viii
List of Abbreviations xi
1. Introduction 1
1.1 Wearable medical devices 1
1.1.1. Human activity monitoring 1
1.1.2. Applications of motion sensing in biomedical devices 2
1.2. Introduction to hydrogels 2
1.3. Application of hydrogels in wearable sensors 3
1.4. Existing challenges of conventional hydrogels 4
1.4.1. Common challenges facing hydrogel design for strain sensing applications 4
1.4.2. Cohesive failure in hydrogels 5
1.4.3. Adhesive failure in hydrogels 6
1.5. Tough hydrogels 7
1.5.1. Chemical crosslinking 7
1.5.2. Physical Interactions 9
1.5.3. Double Network Hydrogels and Interpenetrating Network Hydrogels 12
1.6. Hydrogel Adhesion 13
1.6.1. Interfacial Chemistry and Hydrogel Adhesion 14
1.6.2. Adhesion to Wet Substrates 14
1.6.3. Polyoxometalates 15
1.6.4. Modulating cohesion and adhesion 17
1.7. Conductivity 17
1.7.1. Graphene oxide 18
1.7.2. Ionic Conductivity 18
1.8. Objectives 19
2. Experimental techniques 23
2.1. Methodology for sample preparation and storage 23
2.2. Mechanical properties 24
2.2.1. Stress-Strain Characterization 24
2.2.2. Stress-Strain Curve Analysis 25
2.2.3. Toughness 26
2.2.4. Compression Testing 27
2.2.5. Dynamic Mechanical Analysis 28

2.3. Adhesion properties 29
2.3.1. Tensile adhesion test 30
2.3.2. Probe-pull test 31
3. Synthesis and modulation of adhesion and cohesion in SiW-based hydrogel 34
3.1. Introduction 34
3.2. Materials and Methods 37
3.3. Results and Discussion 41
3.3.4. Adhesive performance 50
3.4 Conclusion 55
4. Application of SiW-based hydrogel in wearable technology and sensing 57
4.1. Introduction 57
4.2. Materials and Methods 60
4.2.1. Materials 60
4.2.2. Synthesis of SiW hydrogel 60
4.2.3. Mechanical properties 60
4.2.4. Transparency 61
4.2.5. Adhesion Testing 61
4.2.6. Electrical Behavior 62
4.3. Results and Discussion 63
4.3.1. Mechanical Properties 63
4.3.2. Adhesion to substrates 65
4.3.5. Rheological Properties and self recovery 72
5. Conclusions and Future Work 74

List of Tables

Table S.1. The compositions of PAM/CMC hydrogels 102

Table S.2. Comparison of PAM/CMC hydrogel to similar hydrogels in literature. 103

List of Figures

Figure 2.1. Schematic diagram of the experimental setup for (a) lap-shear test and (b) probe-pull test. 45

Figure 3.1. Schematic of the synthesis process for the composite hydrogels 54

Figure 3.2. FTIR spectra of SiW compound, PAM, H-0.5-0, and H-0.5-0.5 hydrogels from (a) 2500 cm-1 to 4000 cm -1, (b) 700 cm -1 to 2000 cm -1 56

Figure 3.3. Rheological time sweep of CMC and CMC-SiW. 57

Figure 3.4. (a) SEM image of H-0-0 at 50 μm scale. (b) SEM image of H-0-0m at 20 μm scale. (c) SEM image of H-0-0m at 20 μm scale. (d) Chlorine element mapping in H-0.5-0.5 corresponding to electron image shown in (c). (e) Tungsten element mapping in H-0.5-0.5 corresponding to electron image shown in (c). 58

Figure 3.5. (a) The water content of the as-prepared PAM hydrogel and PAM/CMC hydrogels. (b) The equilibrium swelling ratio of the as-prepared PAM hydrogel and PAM/CMC hydrogels. (c) Lyophilized PAM hydrogel swelling in deionized water for 12 hours and 24 hours. (d) Lyophilized H-0.5-0.5 hydrogel swelling in deionized water for 12 hours and 24 hours. (c) Immersion of PAM hydrogel and H-0.5-0.5 hydrogel (degradation of PAM hydrogel) in deionized water after 48 hours. 60

Figure 3.6. (a) Photos of H-0.5-0.5 before and after elongation on a tensile machine, stretched to 5519 % original length. (b) Tensile stress-stain curves of PAM, H-0-0, H-0.5-0, and H-0.5-0.5 hydrogels. 61

Figure 3.7. True stress, toughness, and Young's modulus of PAM, H-0-0, H-0.5-0, and H-0.5-0.5 hydrogels. 62

Figure 3.8. (a) Photograph of hydrogel sustaining the force of 500g stainless steel weight. (b) Close-up photograph of H-0.5-0.5 hydrogel binding tightly with substrate during tensile adhesion testing. (c) Photographs of lap-shear setup with H-0.5-0.5 hydrogel before and after shearing. 63

Figure 3.9. (a) Lap-shear adhesion strengths of PAM, H-0-0, H-0.5-0, and H-0.5-0.5 hydrogels. (b) Lap-shear adhesion strength of H-0.5-0.5 with varying amounts of MBAA crosslinker. (c) Photos of adhesive failure in H-0.5-0.5 with high crosslinking density. 64

Figure 3.10. Probe-pull adhesion strengths of H-0.5-0.5 hydrogel after immediate attachment, 30s of contact, and 90s of contact. 67

Figure 4.1. Successive tensile tests of H-0.5-0.5 at 100%, 500%, and 3000% strain. (d) Cyclic loading-unloading curves of H-0.5-0.5 hydrogel..... 76

Figure 4.2. (a) Hydrogel and porcine skin entering water separately, attachment of porcine skin to hydrogel in situ underwater, hydrogel stays in place after lifting from water. (b) H-0.5-0.5 hydrogel underwater adhesion to glass. (c) Lap-shear adhesion strength of H-0.5-0.5 on glass, aluminum, NB rubber, polystyrene, and porcine skin substrates in both dry and wet conditions. (d) Probe-pull adhesion strength of H-0.5-0.5 on glass, aluminum, NB rubber, polystyrene, and porcine skin substrates in both dry and wet conditions. 78

Figure 4.3. (a) Electrical conductivities of H-0-0, H-0.5-0, H-0-0.5, H-0.5-0.5. (b) Relative resistance changes of H-0.5-0.5 hydrogel with increasing strain. (c) Cyclic relative resistance changes under repeated finger-bending with a maximum strain of 200 % and 500 %. (d) Real-time sensing performance of hydrogel under touching, tapping, and pressing. (e) Relative resistance changes of the hydrogel under 40 repeated loading/unloading cycles at 100 % strain. 79

Figure 4.4. (a) Photo showing the conductivity of the composite hydrogel by illuminating a LED lightbulb. (b) Photo showing the optical transparency of the hydrogel, scenery shows clearly through the hydrogel. (c) Optical spectra in the visible light range of the hydrogel at 21˚C. The inset picture shows the appearance of the hydrogel. (d) Photo showing composite hydrogel stretching with a knot. 80

Figure 4.5. (a) Decrease in mass and change in lap-shear adhesion strength of PAM, H-0-0, and H-0.5-0.5 hydrogels over time. (b) H-0.5-0.5 (left) and PAM (right) hydrogel after 15 days. (c) Pictures showing pliability of PAM hydrogel and H-0.5-0.5 after 15 days in ambient condition. 82

Figure 4.6. Comparison of the performance of this work to similar reported hydrogels..... 83

Figure 4.7. (a) Rheological frequency sweep measurements of H-0-0 and H-0.5-0. (b) Rheological oscillatory strain sweeps of H-0.5-0.5 hydrogel. (c) Rheological oscillatory strain sweeps of H-1.0-1.0 hydrogel. (d) Cyclic oscillatory time sweep with the shear strain shifting between 1 % and 1000 % for four cycles. (e) Temperature sweep of H-0.5-0.5 hydrogel. 84

Figure S.1. Photograph of as-prepared H-0.5-0.5 hydrogel showing high transparency..... 105

Figure S.2. Self-healing of H-0.5-0.5 hydrogel 104

Figure S.3. H-0.5-0.5 adhesion to a variety of substrates, including porcelain, polypropylene, poly(methyl methacrylate), glass, agate, stainless steel..... 105

List of Abbreviations

AM	Acrylamide
APS	Ammonium persulfate
CMC	Carboxymethyl cellulose
DN	Double Network
ECM	Extracellular matrix
FESEM	Field emission scanning electron spectroscopy
FTIR	Fourier transform infrared spectroscopy
GO	Graphene oxide
GF	Gauge Factor
IPN	Interpenetrating Network
LED	Light emitting diode
MBAA	N, N' methylene bisacrylamide
PAM	Polyacrylamide
PDA	Polydopamine
PEDOT	Poly(3,4-ethylenedioxythiophene)
SEM	Scanning electron spectroscopy
TA	Tannic Acid

1. Introduction

In the epoch of burgeoning technological advancements, the fusion of material science and biomedical engineering is paving the way for innovative solutions in healthcare. Among the myriad of materials explored, adhesive hydrogels have emerged as a focal point of interest, particularly in the realm of wearable sensors. These hydrogels, known for their high water content and adhesive properties, mimic the mechanical characteristics of human tissues, making them an ideal candidate for wearable medical devices. The seamless interface they create with the human skin allows for continuous monitoring and data collection, a feature that is indispensable in today's healthcare landscape.

1.1 Wearable medical devices

1.1.1. Human activity monitoring

The demand for wearable medical devices has experienced a surge in recent times, largely driven by the impact of the COVID-19 pandemic. This has accelerated the transition towards a more digitized and decentralized healthcare system, which has the potential to revolutionize patient care[1-4]. Soft wearable sensors play a critical role in this transition, as they provide real-time data collection and continuous monitoring of health conditions, which is vital in ensuring the quality and timeliness of care[5-8]. By capturing both physical and electrophysiological signals, these sensors have the potential to facilitate early screening and prevention, reduce patient readmissions and enhance care quality through continuous tracking[8-11].

1.1.2. Applications of motion sensing in biomedical devices

The integration of motion sensing technology into biomedical devices has revolutionized the way we monitor and manage our health. In recent years, the development of wearable devices that incorporate this technology has gained significant traction. These devices use sensors to track a user's physical activity and provide real-time feedback, allowing individuals to monitor their fitness levels and make changes to improve their overall health[12]. Motion sensing has also been used to develop rehabilitation devices that can assist patients in regaining mobility following an injury or surgery by monitoring compliance with therapy regimens[13]. Additionally, motion sensing technology has been utilized in the development of devices that can monitor the movement patterns, including gait, in individuals with conditions such as Parkinson's disease, allowing for early detection of potential issues and more targeted treatment[12, 14, 15]. The effectiveness of these wearable devices is enhanced by using a pertinent medium, which translates into higher patient compliance and more accurate results.

1.2. Introduction to hydrogels

Hydrogels are highly versatile materials that are comprised of three-dimensionally cross-linked polymeric networks that have a high water content[13, 16]. The cross-linking process, which serves to retain the water within the gel structure, can be achieved through a range of techniques including intermolecular bonding, ionic bonding, and covalent bonding. Since their discovery by Wichterle and Lim in 1954, hydrogels have been the subject of extensive research and development[17]. The use of hydrogels in various applications has grown significantly in recent years, and their popularity continues to rise due to their unique properties and versatility. Today,

hydrogels are widely used in the medical field, where they are used in wound dressings[18, 19], contact lenses[20-23], and drug delivery systems[24-37].

1.3. Application of hydrogels in wearable sensors

Many conventional conductive materials, such as metals and alloys, suffer from limited flexibility and high Young's modulus, making them ill-suited for use on the skin, particularly on joints where bending angles can exceed 90 degrees. This lack of conformability is a significant barrier for the development of wearable biosensors for human-activity monitoring, which demand a high degree of flexibility and comfort.

Hydrogels that conduct electricity are a promising solution for the development of flexible wearable sensors that can be comfortably worn on the skin[31, 38-42]. Their soft and conformable nature, combined with electrical conductivity, makes them ideal for use as wearable devices that require electrical stimulation or monitoring. For example, hydrogels have been used in the development of wearable sensors for the continuous monitoring of heart rate[38, 43, 44], respiration[45], and other vital signs[46]. The versatility of hydrogels also enables the incorporation of conductive materials, such as conductive polymers or metallic nanoparticles, for electrical signal transmission[47-52]. This creates a range of possibilities for the development of wearable devices that can perform complex monitoring and stimulation tasks.

Despite significant progress in the development of hydrogels, there is still a need for hydrogels that have outstanding performance all around. While a majority of hydrogel research focuses on improving a single property, such as mechanical strength or electrical conductivity, the ultimate goal is to develop a hydrogel that has high performance in multiple areas, including mechanical strength, electrical conductivity, and biocompatibility.

1.4. Existing challenges of conventional hydrogels

1.4.1. Common challenges facing hydrogel design for strain sensing applications

The challenges faced by conventional hydrogels in terms of their use in strain sensing applications are numerous and complex. Firstly, the soft nature of hydrogels is often a drawback when it comes to their use in wearable sensors. As these sensors are required to withstand repeated use and impact, traditional chemically crosslinked hydrogels are not suitable due to their brittle nature[6]. They lack the resiliency required for the sensor to remain functional over time.

Another issue with conventional hydrogels is their lack of energy dissipation upon stretching[53]. Strain sensing requires the material to have a certain degree of stretchability and the ability to dissipate energy, which many hydrogels lack. Therefore, there is a growing interest in developing new methods to produce tough hydrogels, with proven strategies including interpenetrating networks[54], nanocomposites[52], and double networks[25, 55] with covalent and non-covalent networks.

The materials used in the fabrication of hydrogels must be biocompatible and safe for long-term use on the skin. The presence of foreign materials, such as metals or toxic chemicals, can lead to skin irritation, rashes, or even long-term health effects[36, 56, 57].

However, the overall design of a wearable sensor, especially a strain sensor, encompasses more than mechanical strength. It is important for the sensor to have a balance of strength, stretchability, adhesion, water retention, and ionic conductivity which can oftentimes be mutually exclusive properties. The development of hydrogels that are suitable for strain sensing applications, therefore, requires a multi-faceted approach that considers all these factors.

1.4.2. Cohesive failure in hydrogels

Cohesive failure refers to the breakdown of the hydrogel itself and is a challenge to be overcome to ensure the integrity of the material. This is especially prevalent in adhesive hydrogels, as demonstrated in polyacrylamide hydrogels with varying water contents, where the hydrogel network may fail before detachment from the substrate[58]. The challenge in mitigating cohesive failure in hydrogel systems involves engineering a polymeric network with uniform cross-linking density at the molecular level. This can be addressed by examining the interplays of intrinsic work of adhesion, interfacial strength, and energy dissipation in bulk hydrogels[59]. Precise manipulation of polymerization dynamics is crucial, particularly regarding initiator concentration, monomer ratios, and solvent polarity. In studies on fatigue-resistant adhesion of hydrogels, bonding ordered nanocrystalline domains of synthetic hydrogels on engineering materials demonstrated how such nanostructured interfaces can significantly improve fatigue resistance[60]. Nonuniformities in polymerization parameters can result in anisotropic polymer networks, leading to differential mechanical properties and stress concentrations within the hydrogel matrix. The use of double-network hydrogels, combining chemically and physically linked networks, provides insights into achieving high toughness and self-recovery[61]. Such disparities often precipitate localized failure under mechanical loading.

The incorporation of nano-scale fillers (e.g., silica nanoparticles, carbon nanotubes) into hydrogel matrices an emerging strategy to enhance mechanical integrity. These fillers, when uniformly dispersed, can significantly improve the load-bearing capacity and reduce the tendency for cohesive failure by distributing stresses more evenly across the hydrogel structure. For instance, the addition of carbon nanotubes and Al_2O_3 nanoparticles in polymer-derived ceramics is a promising way to enhance the toughness and modulus, resulting in a notable

increase in mechanical properties[62]. The incorporation silica of nanoparticles into hydrogel nanocomposites has garnered significant attention for its ability to increase the elastic modulus beyond the levels achievable by chemical crosslinking alone, indicating a substantial role for these nanoparticles in improving mechanical strength[63].

1.4.3. Adhesive failure in hydrogels

Addressing adhesive failure in hydrogels involves interfacial engineering to ensure compatibility between the hydrogel and the adherend. The central challenge is tailoring the surface chemistry of the hydrogel to promote effective intermolecular interactions with the substrate. Techniques such as surface grafting of polymer chains with specific functional groups (e.g., amine, carboxyl, or thiol groups) are employed to enhance hydrogen bonding or covalent bonding capabilities. Zhao et al. demonstrated the use of nanoparticles-based glues, where surface-activated nanoparticles were integrated with a dissipative hydrogel, forming robust adhesion in seconds to various surfaces without the need for surface pre-treatments. This innovative approach showcases the potential of nanoparticles in enhancing the adhesive capabilities of hydrogels[61].

Additionally, the environmental stability of these bonds under variable conditions like moisture and thermal fluctuations remains a critical concern. Research is currently focused on the synthesis of hydrogels with adaptable surface properties, employing stimuli-responsive polymers that can adjust their adhesion characteristics in response to environmental changes. For instance, Li et al. introduced hydrogel tapes that form strong physical interactions with tissues in seconds and gradually form covalent bonds over hours, using an electrical oxidation technique.

This method, inspired by mussel foot proteins, combines instant and robust wet adhesion with fault-tolerant convenience for biomedical applications[64].

1.5. Tough hydrogels

The development of tough hydrogels by Gong et al. in 2012 was a breakthrough in the field of materials science[65]. The concept of tough hydrogels involves combining the unique properties of hydrogels with those of solid materials to create a composite material that has both the soft and flexible nature of hydrogels and the strength and stiffness of solid materials. Traditional hydrogels are often soft and flexible, and have limited mechanical strength, making them unsuitable for applications that require tough and durable materials. Gong et al. addressed this issue by developing a new type of hydrogel that consists of a soft hydrogel network and a stiff material, such as a polymer or a metal. The stiff material provides the necessary strength and stiffness to the hydrogel, while the soft hydrogel network provides the desired flexibility and high water content. The resulting composite material is tough and resilient, making it suitable for a range of applications, including wearable devices, soft robotics, and advanced biomedical applications.

1.5.1. Chemical crosslinking

Chemical crosslinking in hydrogels refers to the process of covalently bonding polymer chains within a hydrogel network to create a three-dimensional structure. This is achieved through a variety of crosslinking agents or methods, which induce the formation of covalent bonds between polymer chains. The nature of these bonds is permanent and robust, contributing significantly to the mechanical strength and stability of the hydrogel.

In hydrogels, the polymer matrix is typically hydrophilic, enabling the absorption of large amounts of water. The degree of crosslinking in these hydrogels directly affects their physical properties, such as swelling behavior, mechanical strength, and degradation rate. Studies have shown that a higher crosslink density generally results in decreased swelling and increased mechanical strength, but also a decrease in the flexibility and porosity of the material. For instance, research by Annabi et al. on gelatin methacryloyl hydrogels demonstrated that varying the gelatin methacryloyl concentration and degree of methacryloylation can tune properties like water content and mechanical strength[66]. Another study by Khetan et al. evaluated the effects of crosslinking and swelling on polyacrylamide hydrogels, revealing that higher cross-link density led to a higher initial elastic modulus and distinct mechanical properties[67].

The choice of crosslinking agent and method depends on the desired properties of the hydrogel and its intended application. Common methods for chemical crosslinking include the use of bifunctional or multifunctional crosslinkers, such as glutaraldehyde, or the utilization of photo-initiated crosslinking using UV light in the presence of a photo initiator.

1.5.1.1. PAM hydrogels

The chemical crosslinking process is a foundational method for creating network structures in hydrogels by forming chemical bonds between polymer chains. This is particularly evident in polyacrylamide hydrogels, where bisacrylamide is commonly used as a crosslinking agent. For instance, a study on pectin-acrylamide fabricated hydrogels used N, N' methylene bisacrylamide (MBAA) as a crosslinker with ammonium persulfate as an initiator, demonstrating the successful fabrication of stable hydrogels[68].

In a typical process, a solution of acrylamide and bisacrylamide monomers is polymerized using a radical initiator such as ammonium persulfate (APS) and a crosslinking agent, such as MBAA. The radical initiator generates free radicals that initiate the polymerization of the monomers and forms covalent bonds between the acrylamide and bisacrylamide monomers. The crosslinking agent, MBAA, is incorporated into the polymer during the polymerization process, and it links two polymer chains together to form a covalent bond between the acrylamide groups of the two chains, leading to the formation of a three-dimensional network structure[69]. The crosslinking density and properties of the hydrogel can be controlled by varying the ratio of bisacrylamide to acrylamide, the crosslinking agent concentration, the initiator concentration, and reaction time.

1.5.2. Physical Interactions

Physical crosslinking in hydrogels forms a network through non-covalent bonds, such as hydrogen bonds, hydrophobic interactions, ionic bonds, and crystalline structures. Unlike chemical crosslinking, which is characterized by irreversible covalent bonds, physical crosslinking is reversible. These hydrogels have the advantage of being highly responsive to environmental changes, including variations in pH, temperature, and ionic strength[66]. The polymer chains in these hydrogels link through temporary and reversible interactions, endowing the hydrogels with properties such as self-healing and shear-thinning. These features make them particularly suitable for applications in drug delivery and tissue engineering, where ease of use and biocompatibility are critical.

Furthermore, the formulation of these hydrogels is highly adaptable, dependent on the polymer composition and gelation conditions. This adaptability allows for the tailoring of

hydrogels for specific applications, especially in scenarios requiring a predictable response to environmental changes.

1.5.2.1. Polysaccharide Hydrogels and Hydrogen Bonding

Polysaccharide-based hydrogels are a class of hydrogels that are derived from natural polysaccharides such as cellulose, chitosan, alginate, and hyaluronan. These hydrogels have attracted attention due to their biocompatibility, biodegradability, and the ability to mimic the extracellular matrix (ECM) of living tissues.

Chitosan, a cationic polysaccharide derived from chitin, has also been used to create hydrogels. These hydrogels have been shown to have good biocompatibility, biodegradability and are non-toxic and non-immunogenic. Chitosan-based hydrogels have been used for wound healing, tissue engineering and drug delivery[70].

Alginate, a polysaccharide derived from brown seaweed, has also been used to create hydrogels that have been shown to be biocompatible and biodegradable. Alginate hydrogels have been used in a wide range of biomedical applications including wound healing, tissue engineering, and drug delivery[19, 25, 71].

Hyaluronan, a natural component of the ECM, has been used to create hydrogels with good biocompatibility and biodegradability. These hydrogels have been used in a variety of biomedical applications including wound healing, tissue engineering, and drug delivery. In general, the biocompatibility of polysaccharide-based hydrogels is mainly due to their natural origin and inherent biodegradability, and ability to mimic the ECM which is non-immunogenic and non-toxic. However, the biocompatibility of the hydrogels can be further enhanced by introducing functional groups or modifying the hydrogel structure.

Cellulose-based hydrogels are made from one of the most abundant and renewable natural resources on earth, found in the walls of plant cells, and produced by microorganisms. Cellulose has been used to create gels and viscosifiers since the 19th century[72]. Cellulose derivatives such as carboxymethyl cellulose and hydroxyethyl cellulose have been used to create hydrogels with a range of properties and have been used in a variety of biomedical applications due to their biocompatibility[73, 74].

Carboxymethyl cellulose (CMC), another cellulose derivative, has also been extensively researched for biomedical uses[75, 76]. It is recognized as a superior cellulose derivative owing to its polyelectrolyte properties, which make it reactive to variations in pH and ion concentrations. CMC is a water-soluble derivative synthesized by bonding carboxymethyl groups to the anhydro-glucose units present in cellulose, a process that involves the use of chloroacetic acid. It is categorized as an anionic polysaccharide and exhibits superabsorbent qualities, characterized by its significant expansion capacity in response to the electrostatic charges in its polymer matrix. However, its affinity for water can lead to reduced stability when immersed in fluids. This challenge can be addressed by employing crosslinkers to enhance the derivative's structural integrity and stability in aqueous conditions. Suitable crosslinking agents for these cellulose-based hydrogels include, but are not limited to, epichlorohydrin, compounds derived from urea and aldehydes, and various carboxylic acids. Aswathy et al. explored the development of carboxylic acid crosslinked CMC hydrogels, where their physicochemical, morphological, and thermal properties were extensively analyzed to confirm effective crosslinking[77]

In CMC, some of the hydroxyl groups on the cellulose polymer have been chemically modified with a carboxymethyl group. Each cellulose polymer unit in CMC consists of multiple repeating glucose units linked together by beta-1,4-glycosidic bonds. The hydroxyl groups on the

glucose units can be replaced by carboxymethyl groups, as shown in the structure. The degree of substitution refers to the number of hydroxyl groups that are replaced by carboxymethyl groups in the cellulose polymer.

1.5.3. Double Network Hydrogels and Interpenetrating Network Hydrogels

Double network (DN) hydrogels, notable for their dual polymer network structure, have garnered significant attention in polymer science. These hydrogels consist of a tightly crosslinked, rigid first network interpenetrated by a more elastic, loosely crosslinked second network[55, 65]. This configuration endows DN hydrogels with remarkable mechanical properties, such as enhanced strength and toughness, setting them apart from traditional hydrogels.

The mechanical resilience of DN hydrogels stems from their unique network dynamics. Under stress, the rigid network absorbs and dissipates energy through micro-scale breaking, while the elastic network maintains the hydrogel's structural integrity. This synergy not only enables the hydrogels to withstand large deformations but also imparts self-healing capabilities[55, 61, 65, 78]. In biomedical applications, DN hydrogels are particularly promising. Their biocompatibility and mechanical properties make them suitable for tissue engineering, drug delivery, and as artificial cartilage. The versatility of these hydrogels, adjustable by altering the networks' composition and crosslinking densities, allows for customized designs to mimic natural tissue mechanics[79]. Recent research has focused on developing stimuli responsive DN hydrogels, capable of changing properties in response to environmental factors like temperature, pH, or light. These advancements point to a broadened application range for DN hydrogels, reinforcing their potential in creating dynamic and responsive material systems[80].

Interpenetrating network (IPN) hydrogels consist of two or more polymer networks that intertwine physically but are not covalently bonded. Each network is crosslinked in the presence of the other, creating a robust composite material. IPNs combine the mechanical strengths of both networks, leading to improved elasticity, tensile strength, and energy dissipation compared to single-network hydrogels[81]. IPN hydrogels are especially valuable in biomedical applications due to their durable mechanical properties and customizable degradation rates, suitable for tissue scaffolds, wound healing, and drug delivery.

1.6. Hydrogel Adhesion

Adhesion and toughness are often incongruous properties and are difficult to realize in a single material. Tough hydrogels lack adhesion, and vice versa[82]. Non-adhesive strain sensors that are secured by tapes on two ends cannot provide conformal contact to the substrate[46]. To successfully maintain conformal contact to the skin, most hydrogels require a separate adhesive layer, or at least an adhesive coating in order to provide sufficient adhesive force to remain on the skin[83]. The adhesion strength of hydrogels can vary greatly depending on the composition and structure of the hydrogel, as well as the type of substrate it is being applied to.

Strain sensors may use a multilayer approach with separate adhesive and conducting layers[25]. However, this tactic is both complex and runs the risk of separation between layers. Recently, mussel-inspired adhesion polydopamine (PDA) hydrogels have gained attention for endowing hydrogels with self-adhesive properties[84]. Not only do PDA hydrogels demonstrate tissue adhesion, but they also have the ability to adhere to substrates underwater. Unfortunately, there exists evidence suggesting that PDA causes a breakdown in mechanical strength, which is not unimaginable given the form of mussels in nature[84]. Furthermore, catechol-enabled adhesion

has been shown to decrease in strength over time due to the inevitable oxidation of catechol functional groups. It is difficult to achieve a balance between adhesion and cohesion. Indeed, most underwater adhesives take the form of a liquid due to low cohesion strength[85, 86]

1.6.1. Interfacial Chemistry and Hydrogel Adhesion

To enhance adhesion, the interfacial chemistry of the hydrogel must be engineered to promote stronger interactions that can compete with or displace the hydration lubrication effect. This engineering can involve the incorporation of hydrophilic monomers that form hydrogen bonds with the substrate or the use of amphiphilic copolymers that introduce hydrophobic interactions alongside hydrophilic ones to anchor the hydrogel to the surface.

1.6.2. Adhesion to Wet Substrates

Interfacial adhesive interactions in hydrogel systems are often mitigated by the presence of water within the hydrogel matrix, leading to a phenomenon known as hydration lubrication. This effect is critical when considering the application of hydrogels in environments where they must adhere to other surfaces while retaining their intrinsic moisture content, such as in wearable sensors and medical adhesives.

1.6.2.1. Hydration Lubrication Effect

Hydration lubrication is a term that describes the role of bound water molecules in creating a lubricious interface between the hydrogel and the adhering surface. In a typical scenario, the water associated with the polymer network of a hydrogel forms a boundary layer that reduces friction and promotes slippage at the interface, which is a favorable property in reducing wear and tissue irritation for biomedical implants. However, this same property

becomes a substantial obstacle when adhesion is required, as in the case of wearable sensors that must maintain contact with the skin's surface to monitor physiological signals accurately.

The mechanism behind hydration lubrication is rooted in the structuring of water molecules around the polymer chains within the hydrogel. These structured water molecules, often referred to as "hydration shells," are less likely to be squeezed out under pressure compared to free water, leading to a stable, low-friction layer. The water in the hydration shell provides a cushion that allows easy slippage of contacting surfaces over the hydrogel, thus diminishing the interfacial bonding strength and the hydrogel's adhesive capacity.

1.6.2.2. Technical Challenges and Solutions

The challenge is to design a hydrogel that can maintain a strong bond with the skin in wet conditions—such as those encountered with perspiration—while preserving the mechanical integrity and elasticity needed for comfort and movement. Strategies to overcome hydration lubrication involve designing crosslinking networks that permit water to contribute to adhesion through a "water bridge" mechanism, where water acts as a mediator for bond formation rather than as a lubricant.

1.6.3. Polyoxometalates

Silicotungstic acid (SiW) belongs to a unique class of inorganic metal oxides with negatively charged surfaces known as polyoxometalates. Polyoxometalates have complex structures formed from the linkage of metal and oxygen atoms, typically including transition metals such as molybdenum, tungsten, and vanadium. They are effective hydrogen bond donors and interact with polymers, small molecules, and surfactants[87, 88]. Xu et al. demonstrated the

fabrication of adhesive coacervates through the aqueous co-assembly of basic amino acid monomers and SiW[89]. Peng et al. showed that SiW-based coacervates could be used for hemostatic applications owing to their strong adhesive abilities and the compound's inherent antimicrobial properties[9].

SiW's versatility extends to the formation of hydrogels, where its inclusion offers numerous benefits: it can enhance mechanical strength, making hydrogels suitable for load-bearing tasks; it allows for hydrogels with tunable swelling behaviors, adaptable to specific needs; it is biocompatible, which is crucial for medical and biological contexts; and it facilitates the creation of hydrogels capable of controlled drug release, ideal for drug delivery systems. These multifaceted applications highlight SiW's significance in advancing material science and medical engineering.

The incorporation of SiW into hydrogel networks, drawing upon the insights from the adhesive research by Peng et al., could enhance the intermolecular forces between the hydrogel and various substrates. While Peng's study primarily investigated adhesive coacervates, the demonstrated affinity of SiW for hydrogen bonding suggests its potential in hydrogel applications. By adjusting the concentration of SiW within hydrogels, it may be possible to modify the interaction dynamics at the hydrogel-substrate interface, thereby optimizing adhesion. This modification involves a careful balance; the hydrogel must retain adequate water content to preserve its biocompatibility and intrinsic physical properties, while simultaneously enhancing the intermolecular interactions that are crucial for robust adhesion. Although this application of SiW in hydrogels is theoretically plausible based on its observed adhesive properties, empirical studies are needed to confirm its effectiveness and to fine-tune the SiW concentration for optimal hydrogel-substrate adhesion.

1.6.4. Modulating cohesion and adhesion

The strength and failure modes of hydrogel adhesives are closely linked to their internal structure and interaction with substrates. Cohesive failure, the breakdown within the hydrogel itself, is influenced by factors such as chemical composition, crosslinking density, and hydration level. A hydrogel with higher crosslinking density tends to exhibit a stronger internal structure and greater resistance to cohesive failure. Conversely, adhesive failure involves the bond between the hydrogel and substrate. High-adhesion hydrogels commonly detach due to cohesive failure, particularly when the bond strength within the adhesive exceeds that at the adhesive-substrate interface. This tendency for failure within the adhesive, rather than at the boundary, is exacerbated in strong adhesives like epoxies and polyurethanes due to their inherent brittleness and lower energy required for debonding, leading to cohesive rather than adhesive failure[76].

Surface characteristics and mechanical stresses further influence these failure modes. Notably, the conformity of soft adhesives to substrates distributes stress more evenly, potentially reducing adhesive failure risks. The ultimate detachment mode, whether cohesive or adhesive, hinges on the relative strengths of these internal and external bonds.

1.7. Conductivity

Numerous attempts have been made to improve the conductivity of hydrogels for use in wearable devices, with prolific results to date. Most commonly, conductive fillers or polymers such as graphene[8, 11, 24], carbon nanotubes[82, 90-92], polypyrrole[10], and polyaniline[82, 90, 93, 94] are introduced into the hydrogel matrix as a strategy to induce electronic conductivity. These

hydrogels are efficient in transmitting electrical signals but suffer from filler agglomeration and fatigue failure with repeated stretching.

1.7.1. Graphene oxide

The inclusion of graphene oxide (GO) in hydrogels has emerged as a popular method to induce electronic conductivity. GO, known for its high electrical conductivity, large surface area, and single-atom thickness, offers significant potential to enhance the electrical properties of hydrogels. Ren et al. (2019) developed electrically conductive and mechanically tough graphene nanocomposite hydrogels, demonstrating the potential of GO in enhancing both electrical and mechanical properties[95].

However, the integration of graphene oxide into the hydrogel matrix is not without challenges. One notable issue is the tendency for GO particles to agglomerate within the hydrogel, leading to non-uniform conductivity and potentially compromising the hydrogel's structural integrity[96]. Additionally, the presence of graphene oxide can adversely affect the hydrogel's mechanical properties, especially under repeated stretching, often resulting in fatigue failure. Despite these challenges, GO-enhanced hydrogels hold considerable promise in applications requiring high electrical conductivity, such as in biomedical sensors.

1.7.2. Ionic Conductivity

Alternatively, conductivity can be more easily achieved through the addition of ions (e.g. NaCl or LiCl), taking advantage of their inherent solubility in water [42, 97, 98]. Ionically conductive hydrogels offer the advantages of maintaining flexibility and transparency, essential attributes for wearable devices that need to conform to the body without obstructing visibility[96, 98]. This makes them particularly suitable for applications such as strain sensors or health monitors, where these

properties are crucial. However, ionic conductive hydrogels also face their own set of challenges. The stability of ionic conductivity under various environmental conditions and the impact of ions on the hydrogel's swelling behavior and mechanical properties are key considerations. Moreover, ensuring the biocompatibility of these ions when in contact with biological tissues is crucial to prevent adverse reactions.

1.8. Objectives

This study aims to provide a deeper understanding of the dynamic interplay between cohesion and adhesion in hydrogel materials, a topic which is seldom discussed in hydrogel fabrication, and to explore the potential of the SiW-based hydrogel as a promising candidate for advanced healthcare applications, particularly as a versatile component in wearable strain sensors for non-invasive health monitoring. This investigation enables the fine tuning of adhesion and cohesion through the simple addition of SiW to achieve a balance that is optimal for adhesive strain sensors. With an in depth understanding of the interplay of these forces, we have developed a polysaccharide-SiW hydrogel that exhibits a synergistic balance between mechanical toughness and adhesion, facilitated by interfacial hydrogen bonds. This hydrogel demonstrates superior mechanical properties, such as high toughness (20.3 MJ/m^3) and extreme stretchability (4079%), while maintaining robust adhesion to various substrates in both wet and dry conditions. Moreover, the hydrogel's ionic conductivity, enabled by the uniform dispersion of LiCl particles, suggests its suitability for wearable sensor applications that require a durable, conductive interface with human skin. The material conforms to the skin but is also tough due to an interpenetrating network.

The hydrogel is formed by a facile one-pot method, featuring the free radical polymerization of acrylamide (AM) in the presence of Methylenebisacrylamide (MBAA). Chemically crosslinked polyacrylamide (PAM) polymers form the main hydrogel network through countless intermolecular hydrogen bonds. A second interpenetrating network (IPN) consists of carboxymethyl cellulose (CMC), physically crosslinked with SiW. The IPN endows the hydrogel with impressive mechanical properties that are tunable by variation in crosslinking density. Furthermore, the hydrogel displays improved ionic conductivity and water retention ability, allowing for a well-rounded strain sensor that has the potential to enhance overall wearability and encourage user compliance. The result is a uniquely tough, adhesive, and transparent hydrogel with excellent stretchability and water retention ability that can be employed as a wearable strain sensor. Despite the array of attractive properties attributed to the incorporation of SiW, there has yet to be a tough, adhesive hydrogel to take advantage of them.

Chapter 1 presents an in-depth look at wearable medical devices, particularly focusing on human activity monitoring and motion sensing applications. It delves into hydrogels, exploring their use in wearable sensors, challenges faced by conventional hydrogels, and the development of tough hydrogels, including their types and chemical crosslinking methods. The chapter also covers hydrogel adhesion aspects, differences in failure modes, and concludes with a discussion on the conductivity of hydrogels, particularly ionic conductivity, underlining the objectives of this research.

Chapter 2 presents several techniques and methods to evaluate their properties as hydrogel materials and wearable strain sensors, including mechanical properties, frictional properties, adhesion properties,

In Chapter 3 of the thesis, we report the fabrication of a SiW-based hydrogel, and we delve deeply into its adhesion properties and mechanisms. This section will first concentrate on the synthesis of the SiW-based hydrogel and the modulation of its adhesion and cohesion properties. It will begin with a detailed account of the novel one-pot synthesis method, which utilizes free radical polymerization of acrylamide (AM) in the presence of methylenebisacrylamide (MBAA) to create a chemically crosslinked polyacrylamide (PAM) network. The process of integrating carboxymethyl cellulose (CMC) to form a second interpenetrating network, which is physically crosslinked with SiW, will be described. This synthesis approach is notable for its simplicity and efficiency compared to more complex and time-consuming methods used in traditional hydrogel fabrication. Central to this discussion is the role of interfacial hydrogen bonds and the synergistic interaction between components like SiW, PAM, and CMC, which are crucial in facilitating adhesion. A unique feature of this hydrogel, which sets it apart from traditional materials, is its ability to maintain adhesion in both wet and dry conditions. This dual-environment adhesion capability marks a significant advancement over conventional hydrogels and adhesives.

To provide a comprehensive understanding, a comparative analysis with other adhesive materials reported in literature, especially mussel-inspired polydopamine (PDA) hydrogels and traditional catechol-based adhesives reported in literature, is presented. This comparison not only highlights the superior adhesive properties of the SiW-based hydrogel but also underscores its novel applications. Modulation of adhesion and cohesion will be discussed in depth. The tunability of adhesion through variations in composition and cross-linking density is explored, illustrating how this hydrogel can be customized for specific applications across different fields. The discussion will be supported by experimental findings, illustrating the effects of these adjustments on the hydrogel's performance.

Chapter 4 of this thesis focuses on the structural properties, ionic conductivity, and applications of the SiW-based hydrogel, particularly in wearable technology and sensing. This chapter starts with a detailed analysis of the hydrogel's structural composition, emphasizing the dual-network structure of PAM and CMC. This unique structure significantly influences the hydrogel's mechanical properties, including its toughness and stretchability. The role of LiCl and other ions in enhancing the hydrogel's ionic conductivity is then examined, elucidating how this conductivity contributes to its functionality as a sensor in various applications.

The discussion then shifts to the hydrogel's potential in wearable technology, particularly for health monitoring and strain sensing. The hydrogel's ability to conform to skin surfaces and its performance under various environmental and mechanical stresses are highlighted. The section also explores the hydrogel's potential in other sensing applications, considering its unique properties like transparency, stretchability, and adjustable adhesion. Future research directions and potential innovations stemming from the hydrogel's properties are contemplated, with a focus on integrating the hydrogel into existing sensor technologies and exploring new applications in environmental monitoring. Theoretical implications for material science are discussed, particularly in achieving a balance between flexibility, toughness, and adhesion, which is crucial for the development of advanced materials in the field of wearable technology and beyond.

2. Experimental techniques

2.1. Methodology for sample preparation and storage

Hydrogel sample preparation begins with the synthesis phase, where monomers and cross-linking agents are polymerized under specific conditions to achieve the desired chemical composition. Ensuring consistent reaction conditions, such as temperature, pH, and duration, is paramount for uniformity across batches. Post-synthesis, the hydrogel is transferred into molds corresponding to the required shape and size for testing. Commonly, cylindrical molds are employed for mechanical testing purposes. The gelation process, which solidifies the hydrogel, is closely monitored to adhere to the stipulated time and conditions, ensuring the formation of a stable polymer network.

After gelation, certain hydrogels require a curing phase. This phase encompasses additional aging at room temperature. The curing process is pivotal as it can significantly influence the hydrogel's final mechanical and chemical properties. Once curing is complete, hydrogel samples are carefully demolded. The specific conditions of sample preparation will be detailed in later chapters. Storage of hydrogel samples is a critical aspect of the methodology. Immediately post-preparation, hydrogel samples undergo an initial conditioning phase at room temperature to ensure stabilization of their inherent properties. Hydrogels can be sensitive to moisture fluctuations, storage in a controlled humidity environment is essential. This can be achieved using sealed containers. Consistent storage temperature is maintained to avert thermal degradation or alterations in the hydrogel's properties. It's noteworthy that the duration of storage can influence the properties of certain hydrogels, hence samples are utilized within a known stable period.

2.2. Mechanical properties

2.2.1. Stress-Strain Characterization

The stress-strain relationships of the materials are determined using a standard tensile testing machine. Samples are subjected to uniaxial stress, either in the form of stretching or compression. The setup is calibrated to measure the deformation (strain) of the material under applied loads (stress).

Strain Measurement

Tensile strain ε_t is quantified as per Equation 1, where L represents the length of the material under stress and L_0 its initial length. The strain was calculated using the formula:

$$\varepsilon_t = \frac{L - L_0}{L_0} \tag{1}$$

Stress Measurement

Engineering tensile stress, S, also referred to as nominal stress, was computed by dividing the applied force, F, by the initial cross-sectional area, A, of the material, as shown in Equation 2. This measurement assumes a constant cross-sectional area throughout the deformation process.

$$S = \frac{F}{A_o} \tag{2}$$

Given that the actual cross-sectional area of a material typically decreases during elastic or plastic deformation, true stress, σ, was also calculated. This was achieved by adjusting the engineering stress to account for the change in cross-sectional area, as indicated in Equation 3:

$$\sigma = \varepsilon_t S \tag{3}$$

2.2.2. Stress-Strain Curve Analysis

The stress-strain curves were analyzed, focusing on the three distinct regions typically observed. The initial region, characterized by a linear relationship between stress and strain, corresponds to elastic deformation and adheres to Hooke's law. Young's modulus was derived from the slope of this initial linear segment of the stress-strain curve.

Upon reaching the yield point at the end of the elastic region, materials begin to undergo plastic deformation. This transition and the subsequent behavior were carefully monitored and recorded. The final stage of the stress-strain curve, marked by heterogeneous deformation and stress concentration, was also analyzed to understand the material's response under high stress levels.

The classification of the materials into brittle or ductile was based on their behavior under stress, observed through the stress-strain curves. Brittle materials exhibited fracture post minimal elastic deformation and no significant plastic deformation. In contrast, the hydrogels studied, categorized as ductile materials, demonstrated considerable plastic deformation prior to failure.

This methodology provided a comprehensive understanding of the mechanical properties of the materials under study, particularly the hydrogels, in response to uniaxial stress conditions pertinent to their application in wearable sensor technology.

2.2.3. Toughness

Hydrogel Toughness Measurement

Toughness in hydrogels, a crucial mechanical property, encapsulates the material's capacity to absorb energy before fracturing. Defined as the area under the stress-strain curve until the point of fracture, toughness (U) is mathematically represented as

$$U = \int_0^{\varepsilon_f} \sigma(\varepsilon) d\varepsilon_f \tag{4}$$

where $\sigma(\varepsilon)$ denotes stress as a function of strain (ε), and ε_f is the strain at fracture. This integral essentially quantifies the work done per unit volume of the material as it undergoes deformation.

The stress-strain profile of hydrogels typically reveals an initial linear (Hookean) behavior, followed by yielding and non-linear plastic deformation, culminating in fracture. The toughness is thus a product of both the yield strength and the strain at break. It is influenced by factors such as the polymer network structure, where cross-linking density and polymer chain characteristics play pivotal roles. Additionally, the hydrogel's composition, including any fillers or plasticizers, and environmental conditions like temperature, pH, and ionic strength, can significantly modify its toughness.

Experimentally, toughness is determined through tensile or compressive testing, recording the stress-strain data until the hydrogel sample fractures. The area under this curve, calculated via numerical integration, provides a quantitative measure of toughness. This measurement is integral to applications requiring high resilience and energy absorption, guiding the design and optimization of hydrogels for specific uses in fields ranging from biomedical

engineering to soft robotics. Understanding and quantifying toughness is therefore vital in the advancement and application of hydrogel materials.

2.2.4. Compression Testing

The compression testing of hydrogels requires a detailed and systematic approach. The hydrogel samples need to be prepared into uniform cylindrical shapes, with specific attention to maintaining consistent diameters and heights. This uniformity is crucial for ensuring reliable and comparable results across tests.

The testing equipment, a universal testing machine equipped with a compression module should be carefully calibrated to ensure accuracy in force measurement. A critical aspect of the setup was verifying the parallelism of the compression plates, which is essential for the even application of compressive force across the sample.

During the testing procedure, each hydrogel sample is centrally positioned between the compression plates. The compression is applied at a controlled displacement rate, continuing until the sample either reached a predetermined maximum load or exhibited failure. Throughout this process, the force, F, exerted on the sample and the corresponding change in height, Δh, is continuously recorded.

The compressive stress, σ_c, is calculated using the formula:

$$\sigma_c = \frac{F}{A} \tag{5}$$

Where, A, represents the original cross-sectional area of the cylindrical sample, calculated as

$$A = \pi \times \left(\frac{d}{2}\right)^2 \tag{6}$$

The compressive strain, ε_c, is determined by the ratio of the change in height to the original height, expressed as

$$\varepsilon_c = \frac{\Delta h}{h} \tag{7}$$

The compressive modulus, E_c, indicative of the material's stiffness under compression, is derived from the initial linear portion of the stress-strain curve, using the equation:

$$E_c = \frac{\sigma_c}{\varepsilon_c} \tag{8}$$

within the elastic deformation region.

2.2.5. Dynamic Mechanical Analysis

Viscoelasticity characterizes the mechanical behavior of materials that exhibit both viscous and elastic responses under deformation. Viscous components, akin to the behavior of liquids like honey, exhibit a time-dependent strain rate under applied stress. Elastic components, comparable to materials like steel, recover their original shape upon the removal of stress. The viscoelastic properties of materials are quantitatively analyzed using dynamic mechanical analysis, which involves imposing a sinusoidal stress and measuring the resultant strain.

The complex dynamic modulus, G^*, encapsulates the material's viscoelastic response and is defined as:

$$G^* = G' + iG'' \tag{9}$$

Here, i is the imaginary unit. The storage modulus G'quantifies the energy stored and recovered per cycle of stress, indicative of the material's elasticity, while the loss modulus G'' quantifies the energy dissipated as heat, indicative of the material's viscosity.

The relationship between stress, σ, and strain, ε, for the storage and loss moduli can be expressed as:

$$G' = \frac{\sigma_0}{\varepsilon_0} \cos \partial \tag{10}$$

$$G'' = \frac{\sigma_0}{\varepsilon_0} \sin \partial \tag{11}$$

In these equations, σ_0 and ε_0 represent the maximum amplitudes of stress and strain, respectively, while ∂ is the phase angle between the stress and strain waves. The phase angle is a critical parameter, as it provides insight into the relative contributions of the material's viscous and elastic behaviors. A phase angle of 0° indicates purely elastic behavior, while a phase angle of 90° indicates purely viscous behavior. Viscoelastic materials exhibit phase angles between these two extremes. In this way, the viscoelastic nature of materials is thoroughly investigated.

2.3. Adhesion properties

Adhesion in materials engineering is fundamentally governed by the interactions at the interface between two materials. Mechanical adhesion is influenced by the surface roughness, which promotes physical interlocking of surfaces. Chemical adhesion arises from the formation of ionic, covalent, or hydrogen bonds, depending on the reactive groups present on the material surfaces.

Dispersive adhesion is controlled by Van der Waals forces, which are particularly significant in non-polar polymers due to their molecular polarizability. Electrostatic adhesion

results from the attraction between surfaces that carry opposite charges, described by Coulomb's law. In the experimental evaluation of hydrogel adhesion, the methodology rigorously delineates the intermolecular forces and mechanical interlocking phenomena at the hydrogel-substrate interface. The protocol is meticulously crafted to discern the contributions of various bonding mechanisms to the adhesive strength and to parse out the cohesive integrity of the hydrogel matrix.

2.3.1. Tensile adhesion test

The tensile adhesion test method, which measures the force required to separate a hydrogel from a substrate, provides a direct assessment of the adhesive properties. This test is indicative of the combined effects of mechanical interlocking, chemical bonding, and dispersive and electrostatic interactions at the interface. Understanding these adhesion mechanisms is essential for the design and application of materials with specific adhesive characteristics.

The tensile adhesion test commences with the precise preparation of hydrogel samples, ensuring uniformity in composition and geometry for consistency across trials. The tensile adhesion test applies a uniaxial force to the material, typically through a tab or grip. This force is perpendicular to the bond interface and increases until failure occurs. The mechanics of this test involve both the bulk properties of the material and the specific characteristics of the interface.

The force-displacement data are captured to compute the stress-strain relationship, from which the interfacial fracture toughness is derived. This toughness is indicative of the energy per unit area required to propagate a crack along the interface, integrating the effects of mechanical interlocking, chemical bonding, and physical adsorption forces. Mechanical interlocking is assessed by the degree of physical engagement between the hydrogel's polymeric network and

the substrate's surface irregularities. Chemical bonding is evaluated through the potential formation of ionic or covalent bonds and hydrogen bonding, contingent on the functional groups' reactivity on the contacting surfaces. Hydrogen bonds are strong directional bonds that can form between polar groups within the materials and are particularly relevant in hydrogel adhesion.

Ionic and covalent bonds may form at the interface if reactive groups are present and are typically more permanent than Van der Waals or hydrogen bonds. Dispersive adhesion, attributed to Van der Waals forces, is inferred from the adhesion energy in systems where polar interactions are minimal. Van der Waals interactions refer to the weak, distance-dependent forces that are always present between molecules, regardless of the specific chemistry of the material. Electrostatic forces are considered in scenarios where surface charge disparities contribute to the adhesion phenomenon. The tensile adhesion test is thus a macroscopic reflection of these microscopic interactions and provides a measure of the work done against these forces during the test.

2.3.2. Probe-pull test

The probe-pull test isolates the adhesion force at a single point of contact between a probe and the hydrogel surface. The detachment force is measured as the probe is pulled away from the hydrogel, providing a localized assessment of adhesion strength. The critical stress is calculated from the peak load at failure, offering a precise measure of the interfacial adhesion. This test is particularly sensitive to the surface-specific chemistry and the efficacy of any surface treatments, such as silanization, that enhance interfacial bonding. It also gauges the mechanical interlocking effect at the micro-scale, which is accentuated by the probe's sensitivity to surface topography. Additionally, the test can elucidate the extent of molecular interdiffusion, especially

in polymer-substrate interfaces, where polymer chains may interpenetrate to form entangled networks, thereby reinforcing the adhesive bond.

The failure mode analysis post-testing is critical for interpreting the interplay between adhesive and cohesive forces. Adhesive failure indicates a need for improved surface treatment or chemical modification to enhance interfacial bonding, while cohesive failure within the hydrogel suggests that the material's internal strength is the limiting factor in adhesion performance. It provides a direct measure of the strength of the interfacial bond created by the various intermolecular forces. The methodology underscores the importance of a multi-faceted analysis to optimize both the material formulation and the interface engineering for achieving desired adhesion characteristics.

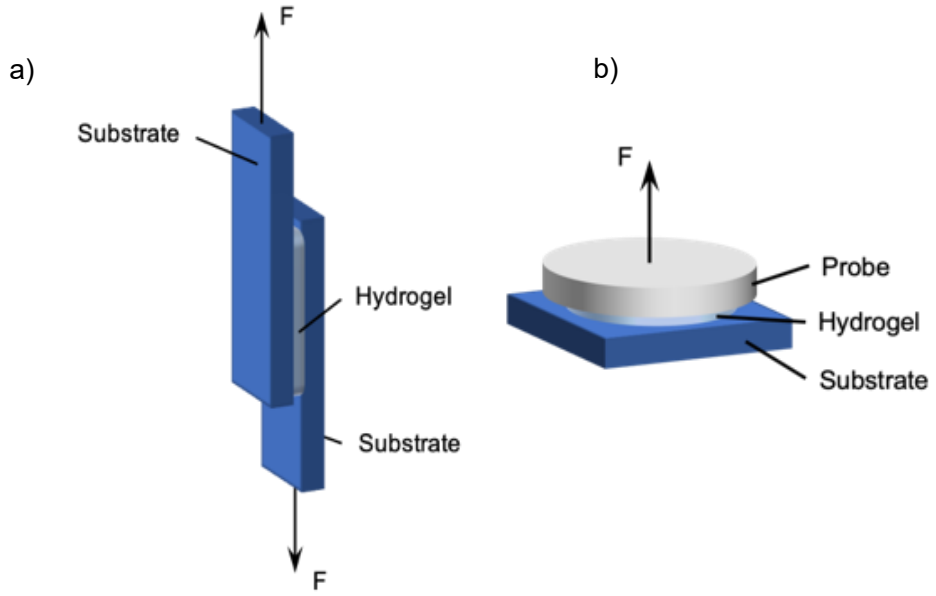

Figure 2.1. Schematic diagram of the experimental setup for (a) lap-shear test and (b) probe-pull test.

In both tests, the failure mode, whether adhesive or cohesive, provides additional information about the nature of the bond. Adhesive failure indicates that the bond at the interface is weaker than the internal strength of the adhesive material, while cohesive failure indicates that the material itself has a lower strength than the interfacial bond.

3. Synthesis and modulation of adhesion and cohesion in SiW-based hydrogel

3.1. Introduction

Hydrogels have become integral in various biomedical applications, offering a means to effectively interface with biological tissues. The customization of hydrogels for specific uses hinges on their cohesive and adhesive properties, which are essential for strong bonding to substrates and maintaining structural integrity under physiological conditions. Just as adhesives are categorized based on their strength and ductility, hydrogels are often designed with a focus on either cohesive strength, which is paramount for their integrity, or adhesion and high water content for bio-integration and flexibility. Modulating the cohesive and adhesive properties is challenging but important for the development of versatile hydrogels that bond well with substrates[99]

Strong cohesion in hydrogels provides a robust framework, yet it often leads to a rigidity that can impair the material's bonding capabilities. This poses a variety of complications, especially to the material's ability to form chemical or physical bonds with a substrate which is vital for adhesion. A higher crosslinking density can limit the availability of functional groups that can interact with the substrate. For instance, if the hydrogel is to adhere through hydrogen bonding or van der Waals forces, a denser network may restrict the mobility of the polymer chains, reducing the opportunity for these interactions. Conversely, the high water content of hydrogels offers flexibility and bio-integration, similar to the ductility of tape adhesives, which prevents abrupt failure by dissipating mechanical stress through a soft matrix, yet this can limit their cohesive strength.

This balance between cohesion and adhesion is exemplified in nature, such as in the adhesive capabilities of marine mussels. This natural adhesion mechanism, integrating covalent and noncovalent interactions, provides valuable insights for synthetic hydrogel design. Marine mussel adhesion, characterized by the integration of covalent and noncovalent interactions, offers a model for synthetic hydrogel design. For example, M. edulis showcases an ability to adhere to diverse substrates under aquatic conditions using a specialized protein matrix. This biological system exemplifies how dynamic bonding mechanisms can result in strong and versatile adhesion. The challenge in hydrogel design lies in emulating such natural paradigms. Naturally derived are preferred over synthetic polymers due to their abundance, biodegradability, and inherent biocompatibility. However, due to their poor crosslinking, biopolymers have little strength or stability under physiological conditions.

Our study aims to overcome this limitation by exploring the modulation of these properties through the incorporation of SiW. As a heteropoly acid, SiW contributes to the hydrogel's adhesion capabilities in moist environments as well - a critical attribute for reliable sensor attachment to human skin. This introduction of SiW into the hydrogel matrix is a crucial development, as it allows for the modulation of adhesion and cohesion properties in a controlled manner, enhancing the material's applicability for continuous health monitoring.

By adopting an interdisciplinary approach to hydrogel design, this study builds upon the extensive investigations into the viscoelastic properties of hydrogels and their significance in enduring repetitive movements. The complexity of SiW hydrogel chemistry is dissected to understand how altering crosslinking density influences mechanical behavior and adhesive properties. Higher crosslinking densities traditionally thought to enhance structural integrity are

reconsidered to avoid compromising the hydrogel's adaptability to skin contours, demonstrating the intricacies involved in designing materials for wearable technologies.

The synthesis process, rooted in a facile one-pot method, leverages the free radical polymerization of acrylamide (AM) with methylenebisacrylamide (MBAA) to form a chemically crosslinked polyacrylamide (PAM) network. This network is further enhanced by a second interpenetrating network of carboxymethyl cellulose (CMC), physically crosslinked with SiW, to create a hydrogel with tunable adhesion and cohesion properties. The introduction will explore the strategic manipulation of interfacial hydrogen bonds to achieve a delicate balance between these properties, which has historically been a complex challenge. By detailing the innovative approach to hydrogel fabrication, this section will set the stage for a comprehensive discussion on the material's synthesis, structural characterization, and the fine-tuning of its mechanical attributes.

In this research, we have meticulously harnessed the potential of SiW to modulate interfacial bonding characteristics, leveraging its high proton conductivity and the ability for tungsten-based coordination with cations to improve the hydrogel's adhesion capabilities. This strategic addition to the hydrogel matrix enhances its mechanical strength without sacrificing the flexibility and transparency needed for practical applications in wearable sensors. The systematic modulation of SiW hydrogels achieves a custom-designed balance of structural integrity and adhesive quality. It addresses the practicality of hydrogels in wearable technology, contributing to the theoretical understanding of SiW hydrogel chemistry and emphasizing practical considerations for a material that meets stringent demands in biocompatibility, mechanical robustness, and environmental stability.

3.2. Materials and Methods

3.2.1. Materials

Acrylamide (AM, 99 %), Sodium Carboxymethylcellulose (CMC, average Mn ~ 90,000), Silicotungstic acid (SiW), ammonium persulfate (APS, 98 %, Aldrich), N, N'-Methylenebisacrylamide (MBAA, 99.5 %) were purchased from Sigma-Aldrich and used as received. Lithium chloride (LiCl, 98.5 %) was purchased from Fisher Scientific and used as received.

3.2.2. Synthesis of SiW hydrogel

Preparation of Hydrogel. In a typical preparation process, 0.6 g of CMC was homogenously dissolved at 50 °C in 8 mL deionized water. Then, varying amounts of SiW were added to the CMC solution at room temperature. AM monomer, along with LiCl salt, MBAA, and APS were added to the mixture and sonicated for 30 minutes. Afterwards, the precursor solution was transferred to a petri dish, sealed, and brought under UV light to undergo free radical polymerization for 50 minutes. A series of hydrogels with varying amounts of SiW, LiCl, and MBAA crosslinker were prepared, which were denoted as H-x-y, with x and y representing the weight percentages of SiW and LiCl, respectively. The detailed contents of the PAM/CMC hydrogels are listed in Table S1.

3.2.3. FTIR and microstructure characterization

The Fourier transform infrared (FTIR) analyses of SiW, H-0-0, and H-0.5-0.5, were performed on a Nicolet iS50 FTIR spectrometer (Thermo Scientific) over a range of 500−4000 cm^{-1} with a resolution of 4 cm^{-1}. The microstructures of PAM, H-0-0, H-0.5-0, and H-0.5-0.5 were measured by scanning electron microscopy (SEM, Zeiss Sigma 300 VP). For analysis purposes, hydrogel samples were lyophilized and coated with gold. The water percentages of composite hydrogels with varying compositions were assessed with their initial weights and their lyophilized weights, with densities defined as the ratio of mass to volume.

3.2.4. Water percentage, equilibrium swelling, and degradation test

To evaluate the swelling behavior of the hydrogel samples, an equilibrium swelling ratio test was also conducted. Initially, the hydrogel samples were dried in a vacuum oven at 40°C until a constant weight (W_d) was achieved. The dimensions of each dried sample were recorded for reference. These dried samples were then submerged in deionized water at room temperature and left undisturbed to swell until equilibrium was reached. The point of equilibrium was determined when consecutive measurements of the sample's weight, taken at regular intervals, showed no significant change. This typically occurred after 24 hours. Once equilibrium was achieved, each sample was carefully removed, blotted gently with filter paper to remove any surface water, and immediately weighed to obtain the swollen weight (W_s).

$$swelling\ ratio = (W_s - W_d)/W_d \times 100\ \% \tag{12}$$

This calculation provided a quantitative measure of the hydrogel's swelling capacity, indicating the extent of water absorption relative to its dry weight.

In parallel, a degradation test in water was performed to assess the stability of the hydrogels. The as-prepared hydrogel samples were initially weighed to record their initial weights (W_i). These samples were then fully immersed in deionized water. At specific time intervals, the samples were retrieved, and excess water was wiped off using filter paper to avoid measurement errors. The weight of each sample at these time points (W_t) was recorded. The relative weight (R_t) of the samples was calculated using the equation:

$$R_t = \frac{W_t}{W_i} \tag{13}$$

This calculation is critical in determining the rate and extent of degradation, as indicated by the changes in relative weight over time. Plotting R_t against time provided insight into the hydrogel's stability and degradation pattern in an aqueous environment.

3.2.5. Rheological characterization

Rheological characterizations were performed on an AR-G2 stress-controlled rheometer (TA Instruments) with a 20 mm 2° stainless steel cone configuration and 53 µm gap. Oscillatory frequency sweep measurements were performed at a strain of 1 %, with the shear rates ranging from 0.1 to 100 rad/s at 35°C to determine the storage and loss moduli of the hydrogels. Strain amplitude sweeps were performed with strain increasing from 0.1 to 2000 % at a constant frequency of 10 rad/s to induce a failure of the hydrogel network, followed by an immediate decrease to 1% strain to observe the effectiveness of network reconstruction. Time-dependent cyclic tests were used to investigate self-healing performances in response to the applied shear stress, with strain alternating continuously between 1 % and 2000 % for a duration of 60s for 5

cycles. The morphologies of the composites were examined using a Zeiss EVO M10 scanning electron microscopy (SEM) at an acceleration voltage of 5 k. The storage (G') and loss (G") moduli were computed from oscillatory frequency sweep measurements conducted at a strain of 1 %, with shear rates varying from 0.1 to 100 rad/s at a controlled temperature of 35°C. G" represents the loss modulus that accounts for the hydrogel's viscous properties, and G' is the storage modulus that reflects the hydrogel's elastic behavior. Following the acquisition of G' and G", the loss factor (tan δ) was computed using the equation.

$$tan\,\delta = G" / G' \tag{14}$$

3.2.6. Mechanical properties

All mechanical tensile tests were conducted at room temperature using an AGS-X universal tensile testing machine (Shimadzu, Japan) equipped with a 50 N load cell. Each sample was trimmed to a rectangular geometry with the dimensions of 12 mm (length) × 10 mm (width) × 2 mm (thickness). The stretching rate employed for the uniaxial tensile tests was kept constant at 50 mm/min. The Young's moduli of the samples were derived from the slope of the stress-strain curve of an initial 15 %. The true tensile stress of the hydrogels was obtained by multiplying the nominal tensile stress with the tensile strain. The toughness of the sample was taken as the area below the nominal stress–strain curves.

3.2.7. Adhesive properties

The adhesive strengths of the hydrogel were tested on a variety of representative substrates using the probe-pull and lap-shear methods. In the lap-shear adhesion tests, the hydrogel samples were sandwiched between two pieces of glass with a bonded area of 10mm by 10mm and

compressed with a 5kPa force for 30s. The glass plates were clamped onto the tensile tester and pulled at 20 mm/min until separation. The adhesion strength was calculated by dividing the measured maximum load by the bonded area. Detachment−reattachment cyclic tests were conducted to evaluate the repeatability of adhesion.

In the probe-pull adhesion tests, a single piece of hydrogel was prepared with a bonded area of 10 mm by 10 mm. The hydrogel was then adhered to a flat substrate surface. A probe was attached centrally to the top surface of the hydrogel. The substrate with the hydrogel attached was secured to the base of the tensile tester, ensuring that the pulling force would be applied vertically. The tensile tester was then operated to pull the probe upwards at a constant rate of 20 mm/min. The force required to detach the hydrogel from the substrate was continuously recorded until complete separation occurred. The maximum load recorded during this detachment was used to calculate the adhesion strength, defined as the maximum load divided by the area of the hydrogel in contact with the substrate. Detachment−reattachment cyclic tests were conducted to assess the repeatability and durability of the hydrogel's adhesive properties.

3.3. Results and Discussion

3.3.1. Design and Fabrication of the SiW Hydrogel.

The adhesive IPN hydrogel system was formed by free radical polymerization of AM in the presence of CMC, SiW, and LiCl, with MBAA acting as the covalent cross-linker. The synthesis process is shown schematically in Figure 1a. The primary chemically cross-linked network is constructed by covalently bonded PAM macromolecules. CMC chains penetrate the PAM network to form a secondary network. CMC is a common water-soluble polysaccharide

featuring functional groups including amino, hydroxyl, and carboxyl groups which can form intermolecular complexation through strong electrostatic and hydrogen bonding interactions between each other. SiW interacts with CMC via hydrogen bonding and heteroatom coordination with the hydroxyl group.[100] These hydrogen bonds can act as sacrificial bonds that break under stress, dissipating energy and thereby preventing catastrophic failure of the material. Upon removal of the stress, these bonds can reform, contributing to the self-healing nature and toughness of the hydrogel. These reversible non-covalent bonds contribute to the toughness and recoverability of the hydrogel.

The addition of LiCl increases the free ion content in the hydrogel to improve conductivity which will be discussed in later chapters. LiCl is a strong electrolyte and therefore has an influence on the conformation of CMC in aqueous solution. Due to the polyampholyte nature of CMC the polymer chains extend from a curled to a stretched conformation, in turn increasing the viscosity of the solution[54, 101]. The extended conformation of the CMC molecular chain allows the formation of additional hydrogen bonds between CMC and PAM, which is beneficial for the overall mechanical properties of the composite hydrogel[54].

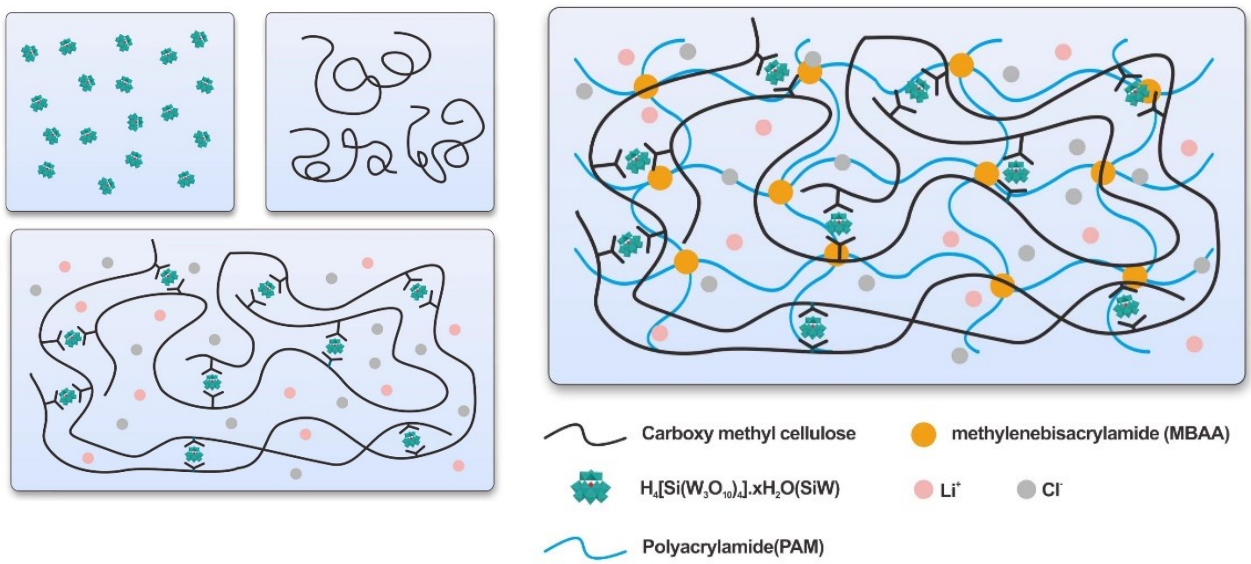

Figure 3.1. Schematic of the synthesis process for the composite hydrogels.

3.3.2. Characterization

The chemical structures of the freeze-dried hydrogels and the individual components were further investigated by Fourier transform infrared (FTIR) spectroscopy (Figure 2a). FTIR spectrum of the pure SiW demonstrates typical stretching vibration bands at 982 cm^{-1} and 922 cm^{-1} corresponding to W=O and Si=O, respectively. In the spectrum of pure PAM hydrogel, the absorption peaks at 1652 cm^{-1} and 1600 cm^{-1} correspond to C=O stretching vibration (Amide I) and N−H bending vibration (Amide II). The spectrums of the freeze-dried PAM, H-0.5-0, and H-0.5-0.5 hydrogel samples show the characteristic peak at 3411 cm^{-1} which derives from the stretching vibrations of the N−H and O−H.

The peaks of 1605 cm^{-1} and 1420 cm^{-1} represent the antisymmetric and symmetrical stretching vibrations of −COO−. The absorption peak of 1061 cm^{-1} ascribes to the CO−H stretching vibration. The FTIR spectrum of the freeze-dried hydrogel shows, too, the representative peaks of antisymmetric and symmetrical stretching vibrations of −COO− at 1417 cm^{-1} and 1608 cm^{-1}, evidencing the presence of CMC in the hydrogel. Moreover, the same stretching vibrations as the ones shown in pure SiW have shifted to 979 cm^{-1}, 919 cm^{-1}, indicating potential interaction between CMC and SiW.

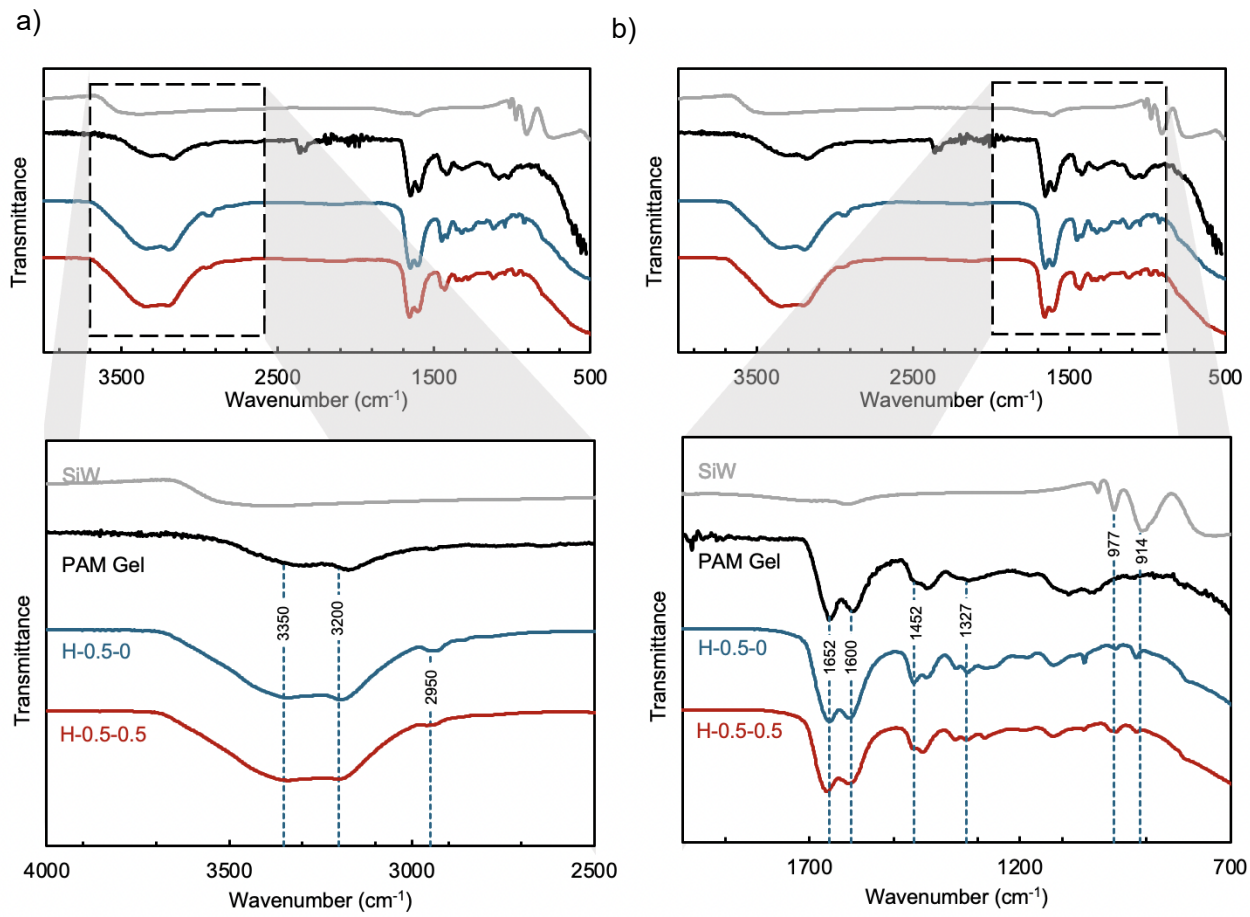

Figure 3.2. FTIR spectra of SiW compound, PAM, H-0.5-0, and H-0.5-0.5 hydrogels from (a) 2500 cm^{-1} to 4000 cm^{-1}, (b) 700 cm^{-1} to 2000 cm^{-1}

To further verify the cross-linking effect of SiW on CMC, CMC-SiW precursor samples were subjected to rheological time sweep to characterize the change in viscoelasticity. As shown in Figure 3.3, the addition of SiW brought the G' and G'' of the sample from 4.9 and 17.4 Pa (where $G'<G''$), to 1210 and 707 Pa ($G'>G''$), i.e. from a fluid state to a gel state.

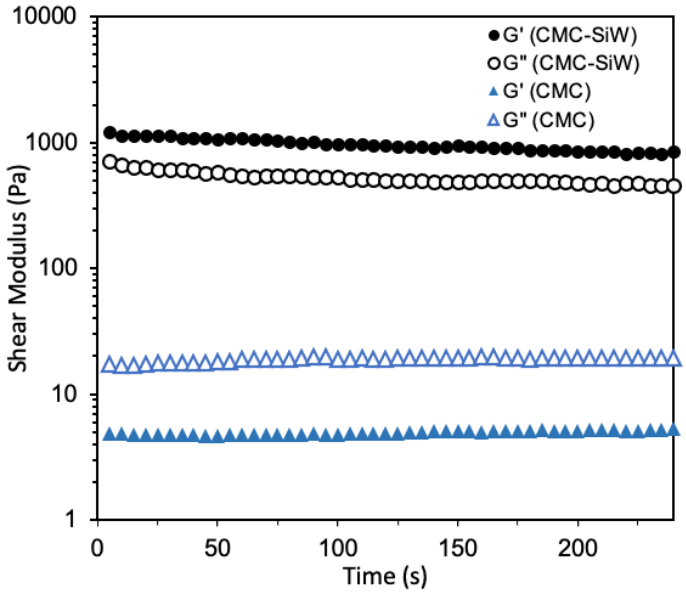

Figure 3.3. Rheological time sweep of CMC and CMC-SiW.

The surface morphology of H-0-0 and H-0.5-0.5 were characterized by FESEM (Figure 3.4). The H-0-0 hydrogel demonstrates a loosely crosslinked homogenous porous structure. The addition of SiW acts like a crosslinker, making the pore number decrease and the density of the network increase, improving the mechanical strength of the sample. Additionally, the pores of the H-0.5-0.5 hydrogel are scattered heterogeneously as opposed to the uniform distribution of the H-0-0 hydrogel, which is relatively uniform, indicating an interweaved three-dimensional structure with the incorporation of SiW.

According to the element mapping in Figure 3.4 d and 3.4 e, silica and chloride ions were homogenously dispersed in H-0.5-0.5, implying the uniform cross-linking of the CMC network. Lithium ions (Li+) from LiCl, due to their small ionic radii and high charge density, are particularly adept at forming strong ion-dipole interactions with the carboxylate groups present

in CMC[102]. This coordination not only disrupts some of the existing hydrogen bonds within the hydrogel matrix but also fosters a more homogenized distribution of SiW[103]. SiW, with its dense array of oxygen atoms, is a key participant in hydrogen bonding. The introduction of Li+ modulates these hydrogen bonding interactions, leading to a more uniform distribution of SiW within the network[103]. This intricate balance between ion-dipole interactions and hydrogen bonding significantly influences the overall network structure and mechanical properties of the hydrogel[102].

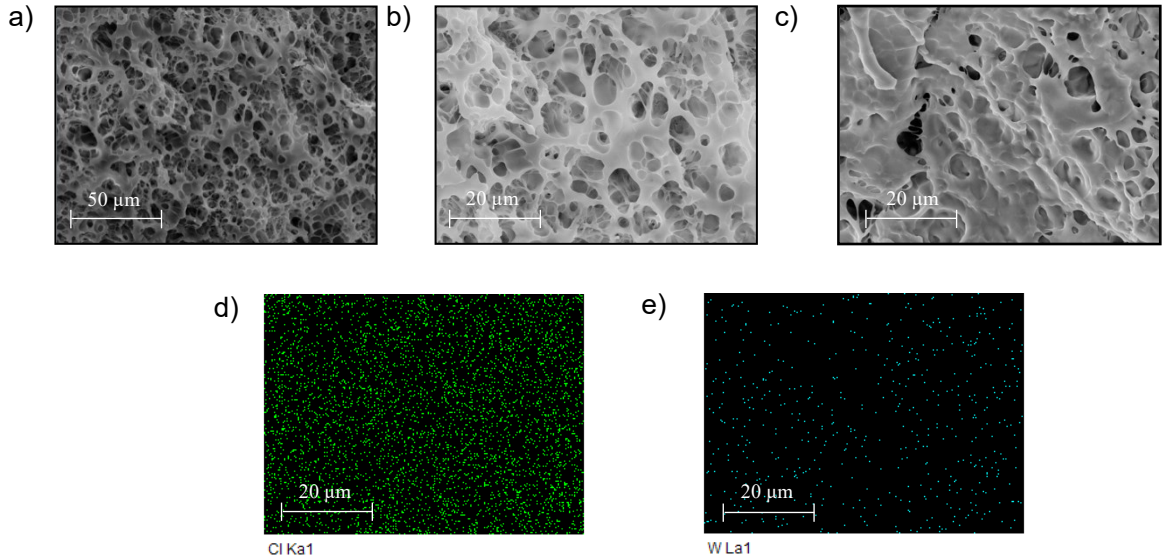

Figure 3.4. (a) SEM image of H-0-0 at 50 µm scale. (b) SEM image of H-0-0m at 20 µm scale. (c) SEM image of H-0-0m at 20 µm scale. (d) Chlorine element mapping in H-0.5-0.5 corresponding to electron image shown in (c). (e) Tungsten element mapping in H-0.5-0.5 corresponding to electron image shown in (c).

The density, water percentage, and swelling ratios of the PAM/CMC hydrogels with varying CMC content (3.9, 4.3, 4.8, 5.2, 5.7, and 6.1 wt%), and varying MBAA content (0.012,

0.016, and 0.018 wt%) were analyzed. The densities of the as prepared hydrogels did not vary significantly with CMC content. The water content of the as prepared PAM/CMC hydrogels decreased accordingly with increased CMC content (Figure 3.5 a). Lastly, the equilibrium swelling ratio of the as-prepared hydrogel decreased with increasing CMC content as the result of increased crosslinking density[104].

The swelling ratio of H-0.5-0.5 was 183 % after submerging under water for 24 hours. On the contrary, the PAM hydrogel expanded a staggering 352 % in the same amount of time. When compared to the lyophilized gels, the PAM hydrogel expanded 1760 %, while the hydrogels with varying amounts of CMC added maintained a relatively stable expansion of around 700 %. The minimal swelling exhibited by the composite hydrogel, as opposed to the significant swelling of polyacrylamide (PAM) hydrogels after 24 hours of submersion in water (Figure 3.5 e), can be attributed to the composite hydrogel's superior crosslinking density and the excellent cohesion within its polymer matrix. The enhanced crosslinking and cohesive forces contribute to a stable network with reduced water uptake, making the composite hydrogel more suitable for applications that demand sustained adhesion and mechanical integrity in aqueous environments.

To further demonstrate the better stability of the as-prepared PAM/CMC hydrogels, a degradation test was conducted for the H-0.5-0.5 hydrogel in water. The relative weight was maintained at under 2.0 indicating that the hydrogel did not degrade in water.

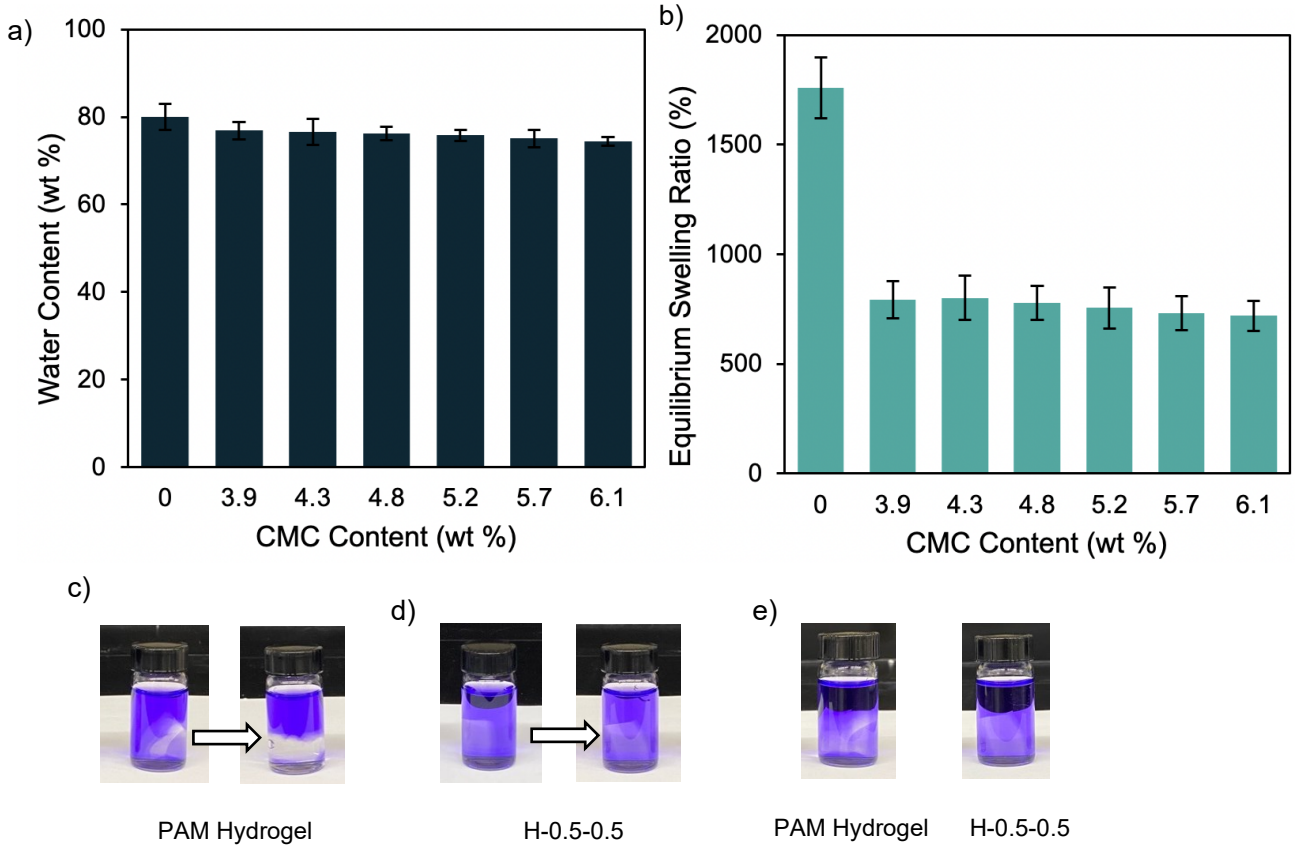

Figure 3.5. (a) The water content of the as-prepared PAM hydrogel and PAM/CMC hydrogels. (b) The equilibrium swelling ratio of the as-prepared PAM hydrogel and PAM/CMC hydrogels. (c) Lyophilized PAM hydrogel swelling in deionized water for 12 hours and 24 hours. (d) Lyophilized H-0.5-0.5 hydrogel swelling in deionized water for 12 hours and 24 hours. (e) Immersion of PAM hydrogel and H-0.5-0.5 hydrogel (degradation of PAM hydrogel) in deionized water after 48 hours.

3.3.3. Mechanical Properties

The mechanical properties of the hydrogels were characterized using a uniaxial tensile testing method. The results from the test are shown in Figure 3.6 b. The pure PAM hydrogel

showed both weak tensile strength and low Young's modulus of 130 and 16 kPa, respectively. PAM/CMC hydrogel showed improved strength (350 kPa) but relatively poor stretchability (1366 %). Incorporating a small amount of SiW increased both the strength (483 kPa) and stretchability (4079 %) of the hydrogel. The PAM/CMC hydrogel with both SiW and LiCl (H-0.5-0.5) showed the highest strength (0.54) and stretchability (5519 %), with a Young's modulus close to that of human skin on the forearm (62 kPa)[100]. Good elasticity was shown prior to slight yielding after 4000% strain which would signify a plastic flow region.

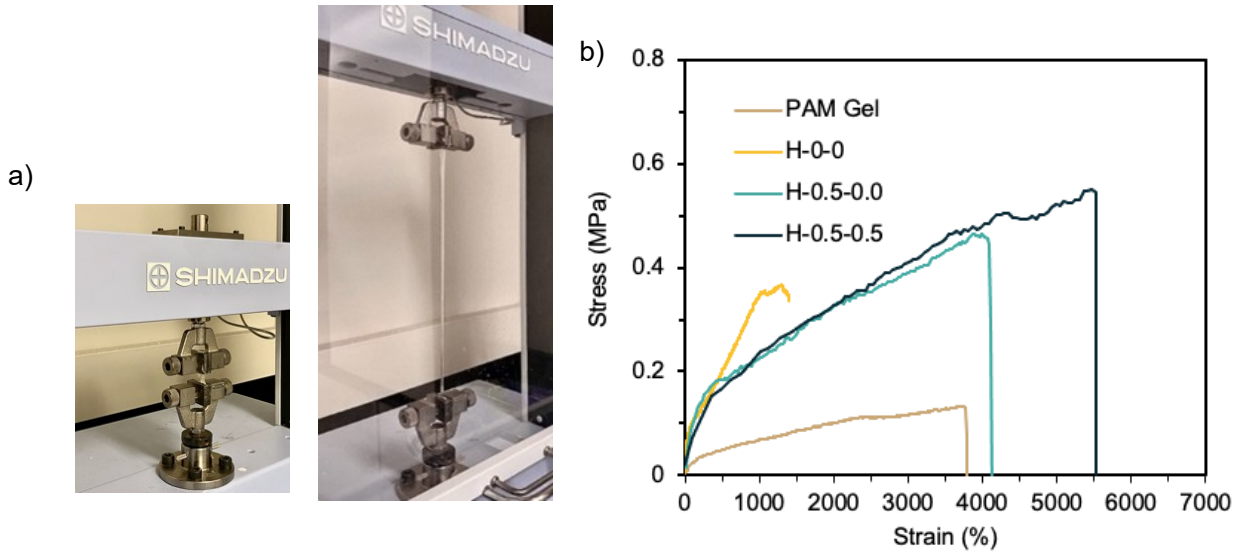

Figure 3.6. (a) Photos of H-0.5-0.5 before and after elongation on a tensile machine, stretched to 5519 % original length. (b) Tensile stress-stain curves of PAM, H-0-0, H-0.5-0, and H-0.5-0.5 hydrogels.

The true stress of the hydrogel was also calculated, as shown in Figure 3.7 e, to account for the decrease in the cross-sectional area with stretching. The true breaking stress calculated for H-0.5-0.5 was 29.8 MPa, six times larger than that of the pure PAM hydrogel. Toughness represents the energy dissipated by unit volume material before breakage. The CMC network

cross-linked by SiW features reversible physical crosslinks, thereby dissipating energy to increase fracture toughness. The composite H-0.5-0.5 hydrogel shows the highest toughness at 20.3 MJ/m^3.

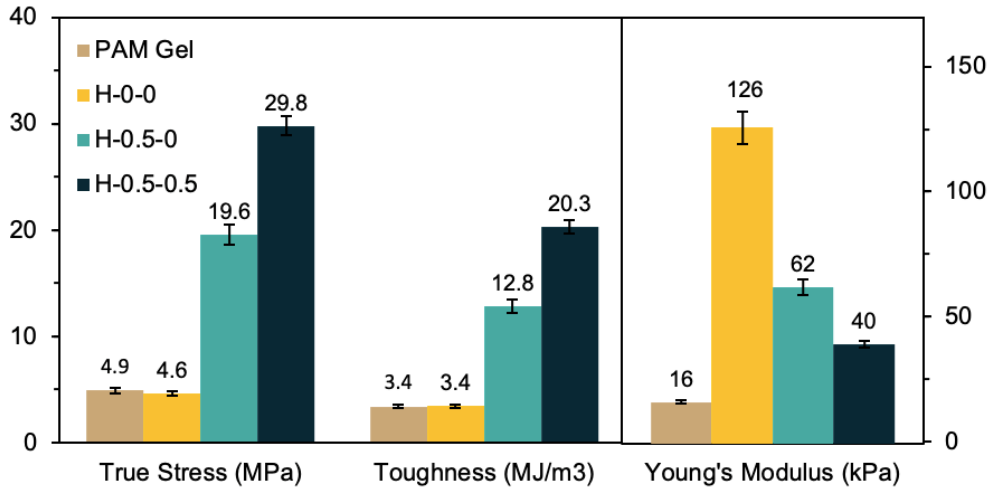

Figure 3.7. True stress, toughness, and Young's modulus of PAM, H-0-0, H-0.5-0, and H-0.5-0.5 hydrogels.

3.3.4. Adhesive performance

Adhesion occurs through the formation of chemical or physical interactions between separate interfaces. Hydrogel adhesion is particularly challenging as its surface is wet, deformable, and contains low densities of bonding moieties. The composite PAM/CMC hydrogel displays outstanding self-adhesive properties to a variety of substrates despite its high water content. The adhesion strength of the PAM/CMC hydrogel to various substrates, including glass, aluminum, copper, rubber, polystyrene, and porcine skin, is governed by a complex interplay of intermolecular interactions such as hydrogen bonding, van der Waals forces, hydrophobic interactions, and mechanical interlocking.

Figure 3.8 a shows the composite hydrogel exhibiting robust adhesion strength, effectively supporting the weight, and maintaining a secure bond, while demonstrating a high load-bearing capacity with minimal deformation or stress. Quantitative evaluation of the hydrogel's adhesive properties for application in wearable strain sensors involved two complementary mechanical testing techniques: lap-shear and probe-pull tests, with glass as a representative substrate. The lap-shear test analyzed the interfacial shear strength between the hydrogel and its substrate, while the probe-pull test examined the adhesive strength under normal stress conditions. Figure 5c shows the experimental setup for lap-shear testing.

Figure 3.8. (a) Photograph of hydrogel sustaining the force of 500g stainless steel weight. (b) Close-up photograph of H-0.5-0.5 hydrogel binding tightly with substrate during tensile adhesion testing. (c) Photographs of lap-shear setup with H-0.5-0.5 hydrogel before and after shearing.

Lap-shear tests were conducted for PAM/CMC hydrogels containing varying amounts of SiW, and MBAA. The lap-shear test of H-0.5-0 exhibited the highest adhesion strength, reaching 72 kPa in its lap-shear test results. H-0.5-0.5 had the second highest adhesion strength at 66 kPa,

followed by H-0-0 and PAM hydrogel which only achieved a 31 kPa and 10 kPa adhesion strength, respectively.

Notably, H-0.5-0.5 with low crosslinking density failed through cohesive failure. H-0.5-0.5 with medium crosslinking density failed through adhesive failure. H-0.5-0.5 with high crosslinking density failed through adhesive failure.

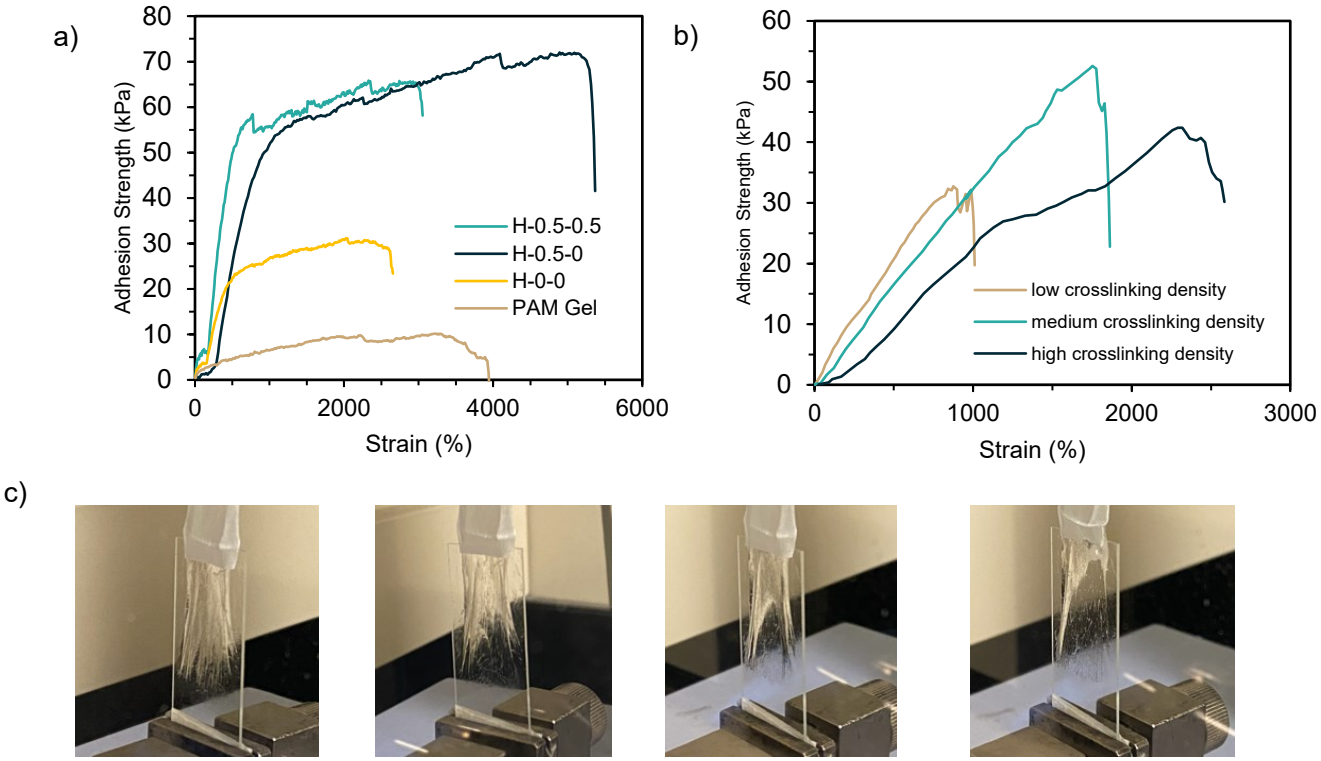

Figure 3.9. (a) Lap-shear adhesion strengths of PAM, H-0-0, H-0.5-0, and H-0.5-0.5 hydrogels. (b) Lap-shear adhesion strength of H-0.5-0.5 with varying amounts of MBAA crosslinker. (c) Photos of adhesive failure in H-0.5-0.5 with high crosslinking density.

To begin, the presence of CMC in the composite hydrogel results in increased viscosity, which is attributed to the stronger cohesive forces between the polymer chains and water molecules due to hydrogen bonding. This enhanced cohesion helps maintain the hydrogel's

structural integrity and stability during the spreading process, allowing it to conform to the substrate surface without compromising its structure. Simultaneously, the adhesive forces between the hydrogel and the glass substrate are bolstered by the hydrogen bonds formed between the carboxymethyl groups of CMC and the hydroxyl (OH) groups on the hydrophilic glass surface. SiW's highly charged and polar structure, which arises from the abundance of oxygen and tungsten atoms, makes it an excellent ligand for coordinating complexes with metal ions on the glass substrate surface. By donating lone electron pairs, the SiW within the hydrogel creates coordination complexes with the glass substrate's metal ions, improving the hydrogel's adhesion. The adhesion strength is not significantly influence by the introduction of LiCl, suggesting the interfacial bonding is mainly hydrogen bonds instead of electrostatic interactions. Collectively, these components work synergistically, creating a robust and interconnected hydrogel structure that facilitates strong interfacial interactions, leading to enhanced adhesion properties crucial for advanced applications.

The adhesion properties of the composite hydrogel can be easily tuned by the degree of chemical crosslinking introduced by MBAA. A balance between flexibility and mechanical strength is achieved at medium crosslinking density, fostering efficient hydrogen bonding and coordination interactions between the hydrogel components and the glass substrate. Both low and high crosslinking densities may compromise adhesion strength due to reduced mechanical strength (cohesion) or limited contact area (due to rigidity), respectively. This understanding of the interplay between crosslinking density and its role on modulating adhesion and cohesion is crucial for designing advanced materials with tailored properties for diverse applications in materials and interfacial science. It is worth noting that while the PAM/CMC hydrogel does not

require curing and is not pressure sensitive, its adhesion strength responds positively to increased contact time.

Figure 3.10 shows the adhesion test results of the H-0.5-0.5 after 0 s, 30 s, and 90 s of contact with the substrate.

The probe pull test, characterized by its localized stress application, primarily captures the adhesive interactions at the probe-hydrogel interface, intensifying the Van der Waals forces, hydrogen bonding, and possible ionic interactions. This localized stress concentration not only amplifies these intermolecular forces but also induces significant deformation within the hydrogel network at the contact point, potentially engaging more elastic chains in the polymer network and thus manifesting in higher adhesion values.

Conversely, the tensile adhesion test, with its more uniformly distributed stress across the hydrogel, tends to reveal the cohesive strength of the material, governed by the same intermolecular forces but over a larger area and with less pronounced deformation-induced intensification. This test, therefore, typically yields lower adhesion values as it reflects the collective intermolecular interactions throughout the bulk of the hydrogel, rather than focusing on the intensified localized interactions at a probe contact point. Such differential outcomes underscore the critical influence of stress distribution and deformation mechanics on the manifestation of intermolecular forces in hydrogel adhesion properties.

For this reason, tensile adhesion testing and probe pull testing are used in unison to provide complementary assessments of adhesion and cohesion.

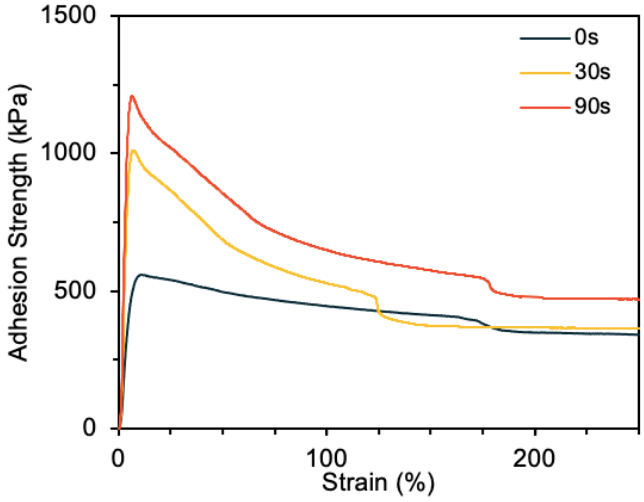

Figure 3.10. Probe-pull adhesion strengths of H-0.5-0.5 hydrogel after immediate attachment, 30s of contact, and 90s of contact.

The adhesion of the composite H-0.5-0.5 hydrogels are enhanced by the introduction of sacrificial hydrogen bonds into the polymer matrix[105, 106].

3.4 Conclusion

In this chapter, we have developed a SiW-based hydrogel, achieving significant progress in the modulation of its cohesive and adhesive properties. Utilizing a one-pot free radical polymerization process, the hydrogel, comprising a PAM/CMC matrix, demonstrated enhanced mechanical properties, with a tensile strength of 350 kPa and stretchability of 1366%. The integration of SiW further improved these properties, resulting in a strength of 483 kPa and stretchability of 4079%. Particularly, the H-0.5-0.5 variant, combining SiW and LiCl, showcased the highest strength of 0.54 MPa and stretchability of 5519%.

The study's success is highlighted by the hydrogel's balanced adhesive and cohesive characteristics. This balance is evident in the lap-shear test results, where H-0.5-0 displayed an adhesion strength of 72 kPa. The ability to modulate these properties was achieved through the careful design of the hydrogel's structure and the inclusion of SiW, which improved bonding within the hydrogel and its interaction with various substrates.

The hydrogel also demonstrated stability in aqueous environments. For instance, the swelling ratio of H-0.5-0.5 was 183% after 24 hours in water, in contrast to a 352% increase in the PAM hydrogel. This suggests a more stable network due to the enhanced crosslinking density, making the hydrogel more suitable for applications requiring consistent adhesion and mechanical integrity in moist conditions.

This research not only enhances the understanding of hydrogel chemistry, particularly for SiW-based hydrogels, but also addresses practical aspects for developing materials for biomedical applications. The approach of combining dynamic covalent chemistry with nanofiller reinforcement sets a new direction for designing advanced soft electronic sensors.

Looking ahead, the potential applications of this SiW-based hydrogel, marked by its optimized mechanical and adhesive properties, are vast. These include health monitoring, disease diagnostics, and soft robotics. Future research in these areas is expected to drive significant advancements in wearable technology and biomaterials, offering innovative solutions for medical and technological challenges.

4. Application of SiW-based hydrogel in wearable technology and sensing

4.1. Introduction

Wearable sensors demand materials that excel in both mechanical compliance and electrical responsiveness. Previous efforts in the domain of soft electronics have laid the groundwork for hydrogels as promising materials for flexible circuits but have frequently grappled with the dichotomy of ensuring conductivity while preserving mechanical flexibility. In the pursuit of materials that replicate the softness, stretchability, and sensory capabilities of human skin, researchers have turned to hydrogels as a promising substrate for wearable sensors. The dynamic nature of skin, with its ability to detect and respond to environmental stimuli such as pressure, strain, and temperature, sets a high bar for artificial materials designed for applications in wearable technology, soft robotics, and health monitoring systems. Traditional hydrogels, while abundant in water and biocompatible, often lack the necessary toughness and elasticity to withstand mechanical stresses or large strains without undergoing plastic deformation. Zhao et al. have highlighted the potential of hydrogels with unconventional polymer networks that provide extreme mechanical properties suitable for durable, skin-like sensors. Calvert's conceptualization of blending softness with electronic functionality in hydrogel design resonates with the development of ionic conductive hydrogels that simulate skin's flexibility and sensory perception. These wearable hydrogel sensors have broadened the potential for wearable sensors that require a delicate balance between mechanical integrity and electrical responsiveness.

The design of materials suitable for wearable sensors demands a delicate balance between mechanical compliance and electrical sensitivity. Zhang and Khademhosseini's advancements in

engineering hydrogels provide a foundation for optimizing these materials for seamless integration with biological tissues, ensuring that the ideal material possesses the ability to endure physiological movement and external mechanical forces while providing accurate sensory feedback. Additionally, in the design of an adhesive sensor, it is important the modulus of the material is similar to that of the substrate, as discrepancies in the moduli can generate interfacial stresses which result in bond failure. When interfacing with skin, soft, flexible and stretchable materials that have similar moduli to skin are preferred [107, 108].

SiW hydrogels, with their intrinsic ionic conductivity and viscoelasticity, satisfy these requirements owing to their unique composite structure. In this chapter, we dissect the application potential of SiW hydrogels, emphasizing their utility in wearable technology where sensorial feedback and user comfort are paramount. By exploiting the high proton conductivity of SiW and the added LiCl, these hydrogels are tailored for wearable sensors, providing an interface that is highly conductive yet remain soft, flexible, and mechanically unobtrusive. SiW, AM, and CMC concentrations in the hydrogels are meticulously tuned to harmonize for optimal sensor performance.

In wearable sensor design, the material's ability to endure and functionally respond to physiological movement and external mechanical forces is crucial. This requires a robust material that can recover from deformation, sustain repeated usage, and resist fatigue - criteria met by the dynamic crosslinking properties of the SiW hydrogel network. The dynamic physical bonds formed between the polymer chains provide a mechanism for energy dissipation and contribute to the material's toughness. The resilience of the hydrogel is further enhanced by the incorporation of SiW, which, through its polyoxometalate clusters, adds to the network's ability to dissipate mechanical stress via reversible ionic crosslinking and tungsten-oxygen bond

formations. This unique interplay of intermolecular forces within the SiW hydrogel matrix is critical for developing wearable sensors that can adapt to the body's topography and movements. The presence of tungsten (W) atoms within the Keggin unit of SiW allows for coordination with various cations, which can be exploited to create interfacial linkages with biological substrates.

In this investigation, we have fabricated a novel SiW hydrogel that exhibits superior elasticity, stretchability, self-healing, and stimuli-responsive properties, combined with exceptional ionic conductivity. This hydrogel, synthesized via a one-pot free radical polymerization of acrylamide (AM), carboxymethyl cellulose (CMC), and silicotungstic acid (SiW), leverages the intrinsic properties of its constituents to establish a robust, responsive matrix. The AM component is integral to forming a strong polymeric backbone through its network of intermolecular hydrogen bonds, while CMC, known for its hydrophilic nature, contributes to the hydrogel's moisture management and enhances its mechanical compliance. SiW is strategically incorporated for its dual role: it reinforces the hydrogel network's structural integrity and contributes to its adhesion and sensing capabilities through strong electrostatic and hydrogen bonding interactions with the CMC chains.

The optimized SiW-PAM-CMC hydrogel was rigorously tested, displaying excellent mechanical properties, such as rapid recovery from extensive stretching and compression, and maintaining structural fidelity after damage. Its application potential was further validated as a transducer for wearable sensor devices, where it demonstrated highly sensitive detection of both macro- and micro-movements, attributed to its finely tuned network properties. The resulting sensor performance suggests a significant advancement over existing hydrogel-based sensors, positioning the novel SiW hydrogel as a leading material for next-generation wearable technology and electronic skin applications.

4.2. Materials and Methods

4.2.1. Materials

Acrylamide (AM, 99 %), Sodium Carboxymethylcellulose (CMC, average Mn ~ 90,000), Silicotungstic acid (SiW), ammonium persulfate (APS, 98 %, Aldrich), N, N'-Methylenebisacrylamide (MBAA, 99.5 %) were purchased from Sigma-Aldrich and used as received. Lithium chloride (LiCl, 98.5 %) was purchased from Fisher Scientific and used as received.

4.2.2. Synthesis of SiW hydrogel

Preparation of Hydrogel. In a typical preparation process, 0.6 g of CMC was homogenously dissolved at 50 °C in 8 mL deionized water. Then, varying amounts of SiW were added to the CMC solution at room temperature. AM monomer, along with LiCl salt, MBAA, and APS were added to the mixture and sonicated for 30 minutes. Afterwards, the precursor solution was transferred to a petri dish, sealed, and brought under UV light to undergo free radical polymerization for 50 minutes. A series of hydrogels with varying amounts of SiW, LiCl, and MBAA crosslinker were prepared, which were denoted as H-x-y, with x and y representing the weight percentages of SiW and LiCl, respectively. The detailed contents of the PAM/CMC hydrogels are listed in Table S1.

4.2.3. Mechanical properties

All mechanical tensile tests were conducted at room temperature using an AGS-X universal tensile testing machine (Shimadzu, Japan) equipped with a 50 N load cell. Each sample was trimmed to a rectangular geometry with the dimensions of 12 mm (length) × 10 mm (width) × 2 mm (thickness). The stretching rate employed for the uniaxial tensile tests was kept constant at 50 mm/min. The Young's moduli of the samples were derived from the slope of the stress-strain

curve of an initial 15 %. The true tensile stress of the hydrogels was obtained by multiplying the nominal tensile stress with the tensile strain. The toughness of the sample was taken as the area below the nominal stress–strain curves.

To measure the time-dependent recoverability of the hydrogel, the samples were pulled to 1000 % strain and then unloaded. After storage for varying amounts of time (0s, 10s, 1min, 5min), the sample was pulled to 1000 % strain again to measure recovery of mechanical strength. To measure elasticity, cyclic tensile tests were performed at a constant stretching rate of 50 mm/min to predetermined strain rates of 100 %, 500 %, 1000 %, and 3000 % for 20 cycles with 0s wait time between cycles. Compression tests were performed on cylindrical hydrogel specimens with diameters of 17 mm and a height of 10 mm.

4.2.4. Transparency

The transparency of the hydrogels was measured using ultraviolet visible (UV-Vis) spectroscopy with a Thermo Evolution 300 UV-Vis machine. The hydrogel sample was prepared with a thickness of 3 mm.

4.2.5. Adhesion Testing

The adhesive strengths of the hydrogel were tested on a variety of representative substrates using the probe-pull and lap-shear methods. In the lap-shear adhesion tests, the hydrogel samples were sandwiched between two pieces of substrate with a bonded area of 10mm by 10mm and compressed with a 5kPa force for 30s. The substrate being tested against was mounted on glass plates that were clamped onto the tensile tester and pulled at 20 mm/min until separation. The adhesion strength was calculated by dividing the measured maximum load by the bonded area. Detachment–reattachment cyclic tests were conducted to evaluate the repeatability of adhesion.

In the probe-pull adhesion tests, a single piece of hydrogel was prepared with a bonded area of 10mm by 10mm. The hydrogel was then adhered to a flat substrate surface. A probe was attached centrally to the top surface of the hydrogel. The substrate with the hydrogel attached was secured to the base of the tensile tester, ensuring that the pulling force would be applied vertically. The tensile tester was then operated to pull the probe upwards at a constant rate of 20 mm/min. The force required to detach the hydrogel from the substrate was continuously recorded until complete separation occurred. The maximum load recorded during this detachment was used to calculate the adhesion strength, defined as the maximum load divided by the area of the hydrogel in contact with the substrate. Detachment–reattachment cyclic tests were conducted to assess the repeatability and durability of the hydrogel's adhesive properties.

4.2.6. Electrical Behavior

Electrochemical impedance spectroscopy conducted using a digital source meter (CHI920, CH Instruments, USA) was used to obtain the electrical conductivities of the composite PAM/CMC hydrogels. A frequency range of 10^{-1} to 10^{6} and an open circuit voltage of 5mV were employed. The conductivity was calculated using the equation:

$$\sigma = \frac{L}{R_b S} \tag{15}$$

Where L is the gauge length of the hydrogel sample (m), S is the cross-sectional area (m^2), and R_b is the bulk resistance. Real-time I-t (current vs. time) tests were conducted to measure the relative current changes during stretching and applied pressure. The results from the test can be converted to resistance change with the following equation:

$$\frac{\Delta R}{R_0} = \frac{I_0}{I} - 1 \tag{16}$$

Where ΔR is the change in resistance, R_0 is the initial resistance, and I_0 is the initial current. The sensing performance of the hydrogel was evaluated based on common human motions such as finger, wrist, and elbow bending, and physiological signals such as breathing and wrist pulse. For motion sensing, the hydrogel sample size was kept consistent at 30mm length, 10mm width, and 1mm thickness.

4.3. Results and Discussion

4.3.1. Mechanical Properties

Exposing a hydrogel sample to a cyclic load leads to fatigue damage to certain mechanical properties, such as the elastic modulus. The fatigue damage of PAM/CMC hydrogels was measured by cyclic tensile tests and shown in Figure 3b. The composite hydrogel saw a complete recovery after applying a maximum loading strain of 100 % and 500 %. At an extremely high strain of 3000 %, energy dissipation mechanisms came into play, and the hydrogel showed hysteresis in the second and third cycles. The remaining cycles showed good superposition, an indicator that broken hydrogen bonds are rapidly rebuilt during the unloading process. The composite PAM/CMC hydrogel was able to restore 92 % of its original shape and 90 % of its strength at the 3rd cycle, indicating outstanding elasticity compared to previous literature. Figure 3d shows the hydrogel under compression. When three cycles of 90% compressive strain are applied, the loading/unloading curves overlap completely, suggesting a full recovery of the hydrogel network. In the loading/unloading process, the PAM network provides elasticity while the reversible hydrogen bonds between the amide groups on PAM

chains and groups on CMC chains, and the physical bonding between SiW and CMC readily break upon loading.

The influence of SiW and LiCl concentrations on tensile stress, strain, and toughness was also investigated. It is worth noting that SiW and LiCl salt concentrations were limited by their solubility in the precursor solution. As the amount of SiW increases, the number of ionically crosslinked bonds per unit volume increases as well, thereby increasing the toughness of the hydrogel. Increasing the LiCl concentration up to 0.5 wt % improves the toughness of the hydrogel from 12.8 to 20.3 MJ/m3. This phenomenon aligns with the assumption that the introduction of LiCl shields the charges on the CMC chains, allowing the extension of the curled conformation, which in turn creates more topological entanglements and increases the contact of the side groups between CMC and PAM chain. The concentration of LiCl was less effective on the modulus of the hydrogel as the modulus is largely dependent on the continuous PAM network. Crosslinker concentration impacts the mechanical properties of the composite hydrogel. With the increase in MBAA, fracture stress and Young's modulus also increases. Varying MBAA concentration endows the hydrogel with tunable mechanical properties.

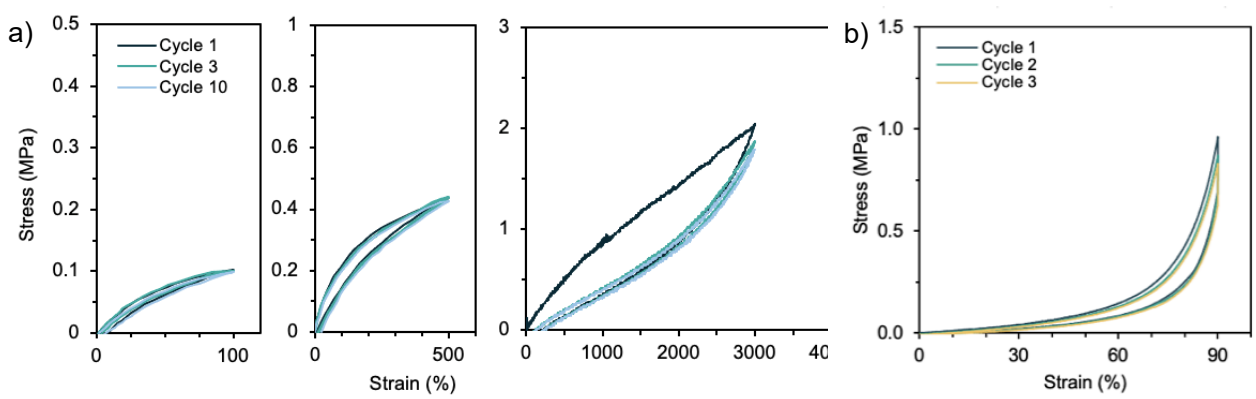

Figure 4.1. Successive tensile tests of H-0.5-0.5 at 100 %, 500 %, and 3000 % strain. (d) Cyclic loading-unloading curves of H-0.5-0.5 hydrogel

4.3.2. Adhesion to substrates

To examine the effectiveness of adhesion on biological tissues, porcine skin was used in lap-shear tests to imitate the condition of human skin. The SiW hydrogel was able to adhere to not only a sheet of glass, but also porcine skin while fully submerged in water (Figure 4.2 a) and could generate an adhesion strength of 20 kPa on dry porcine skin (Figure 4.2 c). Furthermore, the ability for the hydrogel adhere to human skin under practical conditions was tested. The hydrogel could resist being washed away under the strong flow of running tap water (Supporting Video 1). The outstanding skin adhesion properties of the SiW hydrogel can be attributed to the hydrogen bonding interaction between SiW and −NH2, −OH groups on human and porcine skin. Lap-shear tests of H-0.5-0.5 on different substrates under dry and wet conditions were conducted, and the results are summarized in Figure 4.2 c. Measurements on wet substrates was achieved by submerging the substrate in water for 10 s prior to loading on the tensile machine. Surprisingly, the hydrogel showed stronger adhesion strength to glass while it was wet (79 kPa) versus when it was dry (73 kPa). The wet and dry adhesion strengths between the composite and metal surfaces did not vary drastically. On aluminum and copper substrates, the adhesion strengths were 43 kPa and 41 kPa, respectively when dry, 38 and 40 kPa when wet. On NB rubber, polystyrene, and porcine skin substrates, the presence of water negatively affected lap-shear adhesion strength. According to these results, wetting the substrates may enhance adhesion to glass and metals through facilitated hydrogen bonding, while the adhesion strength to porcine skin may be influenced by the balance of promoted hydrogen bonding and weakened hydrophobic and van der Waals interactions. However, for hydrophobic substrates like rubber and polystyrene, water could reduce adhesion strength by disrupting van der Waals forces, hydrophobic interactions, and introducing a hydration layer.

Probe-pull adhesion tests for H-0.5-0.5 were conducted on various substrates under both dry and wet conditions, offering a complementary perspective to the lap-shear test results illustrated in Figure 4.2 d. Notably, the probe-pull tests yielded adhesive strength values nearly ten times higher than those observed in the lap-shear tests. This discrepancy can be attributed to the differences in force application and distribution between the two testing methods. Probe-pull tests apply a localized, concentrated force on the hydrogel-substrate interface, emphasizing the role of surface chemistry and topography in adhesion performance, lap-shear tests involve a more distributed force, highlighting the influence of bulk material properties and interface conformability.

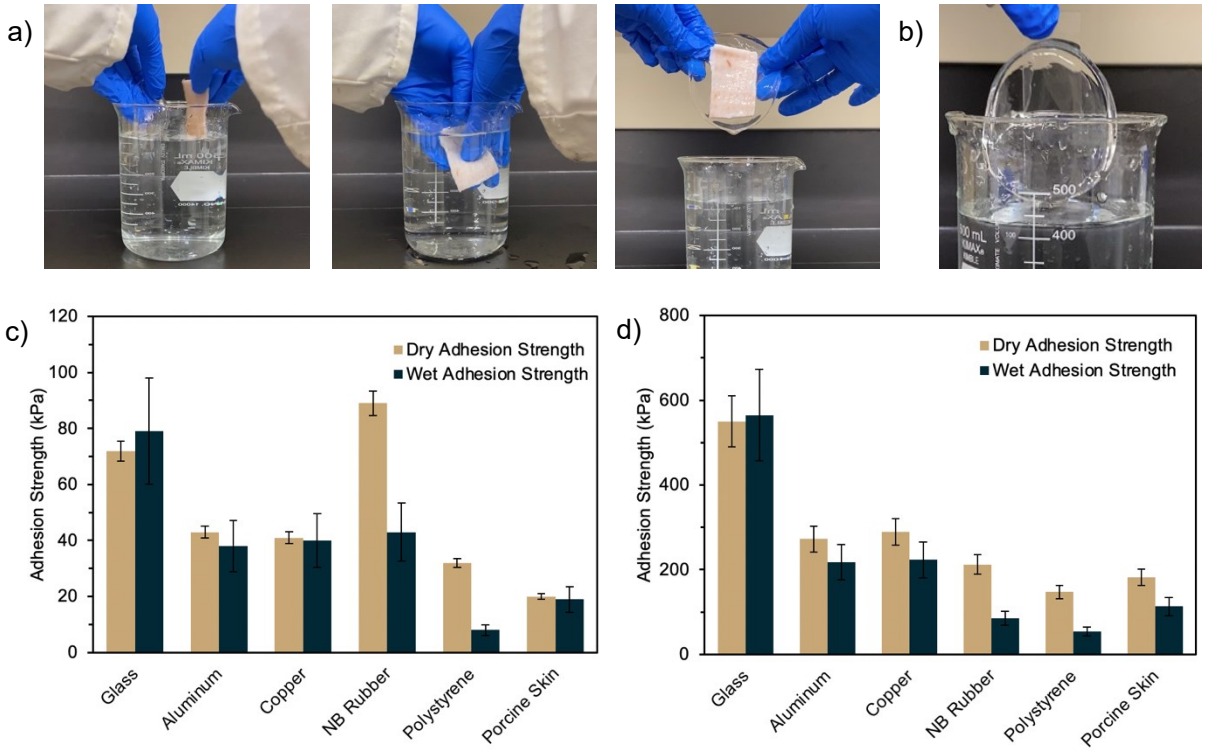

Figure 4.2. (a) hydrogel and porcine skin entering water separately, attachment of porcine skin to hydrogel in situ underwater, hydrogel stays in place after lifting from water. (b) H-0.5-0.5 hydrogel underwater adhesion to glass. (c) lap-shear adhesion strength of H-0.5-0.5 on glass, aluminum, NB rubber, polystyrene, and porcine skin substrates in both dry and wet conditions.

(d) probe-pull adhesion strength of H-0.5-0.5 on glass, aluminum, NB rubber, polystyrene, and porcine skin substrates in both dry and wet conditions.

Furthermore, hydration lubrication in hydrogels involves the structuring of water molecules around polymer chains, creating a low-friction layer beneficial for biomedical applications like implants but challenging for applications needing strong adhesion, like wearable sensors. The stability and fluidity of this layer under pressure are due to its fast molecular exchange rate with surrounding water, enhancing lubrication but reducing adhesive capacity[109]. As such, hydrogel design must not only overcome contending adhesive and cohesive properties, but also have the ability to adhere to wet substrates.

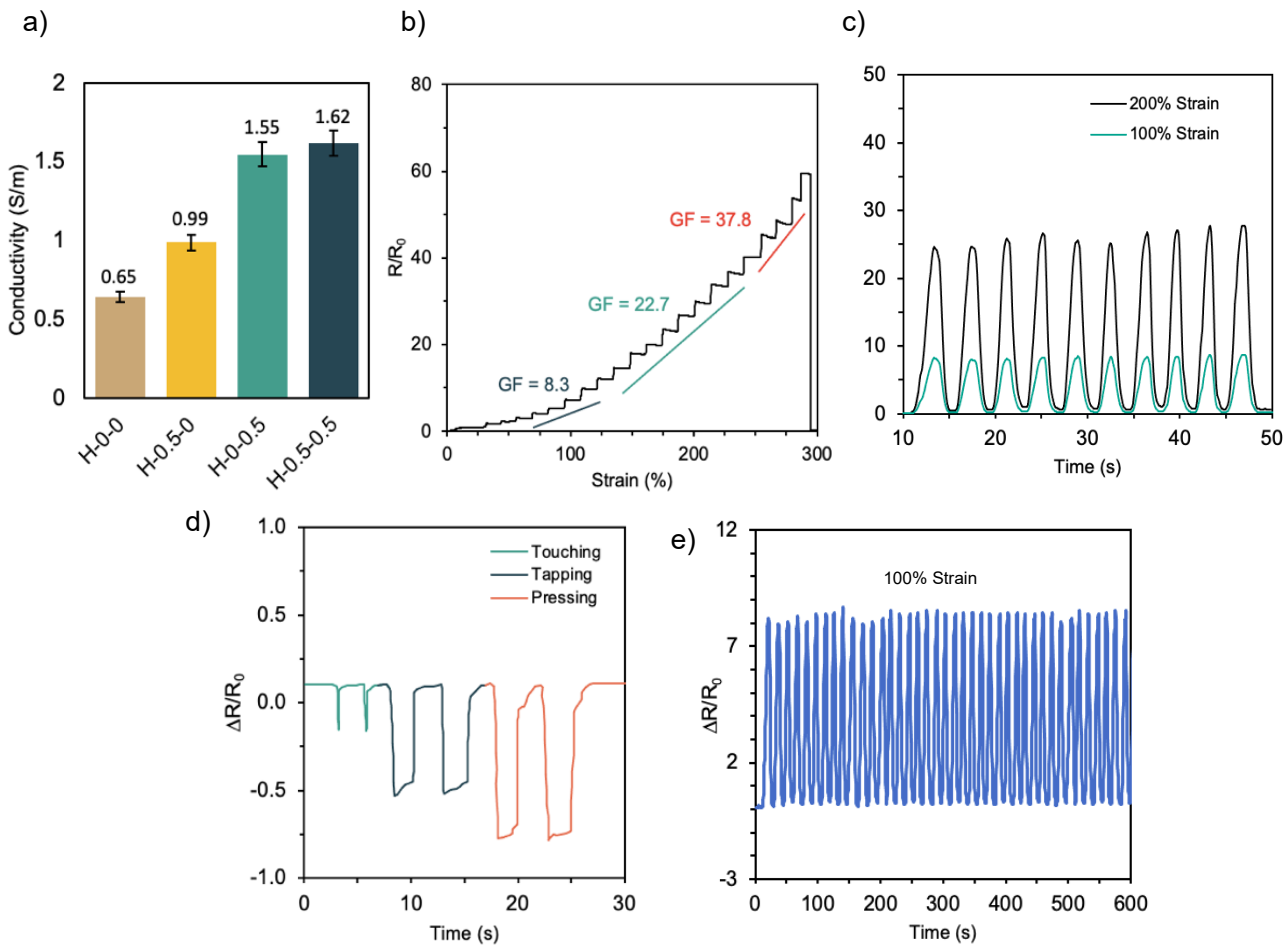

Figure 4.3. (a) Electrical conductivities of H-0-0, H-0.5-0, H-0-0.5, H-0.5-0.5. (b) Relative resistance changes of H-0.5-0.5 hydrogel with increasing strain. (c) Cyclic relative resistance changes under repeated finger-bending with a maximum strain of 200 % and 500 %. (d) Real-time sensing performance of hydrogel under touching, tapping, and pressing. (e) Relative resistance changes of the hydrogel under 40 repeated loading/unloading cycles at 100 % strain.

LiCl dissolved in solution provided free ions that could transport electric charge and enhance ionic conductivity in the hydrogel. The conductivities of the hydrogels were measured using an electrochemical workstation and calculated from the electrochemical impedance spectra. Figure 4.3. a shows the conductivities of H-0-0, H-0.5-0, H-0-0.5 and H-0.5-0.5, highlighting the effect of individual components on the overall electrical conductivity of the hydrogel. The addition of LiCl ions visibly enhanced the conductivity of the hydrogel to 1.62 S/m, a 0.97 S/m increase from the PAM/CMC hydrogel which does not contain any ions. As shown in Figure 4.4.a, a current passing through the sample can light a red LED bulb. At 6 wt.% CMC, the hydrogel still maintains optical transparency (Figure 4.4. b), with a transmittance of over 90% under visible light (Figure 4.4. c). The resulting hydrogel is sufficiently tough to withstand large deformations such as cutting with a sharp blade, knotting (Figure 4.4. d), and compression without any damage. The excellent resistance to damage signifies a well-crosslinked 3D network with effective energy dissipation mechanisms.

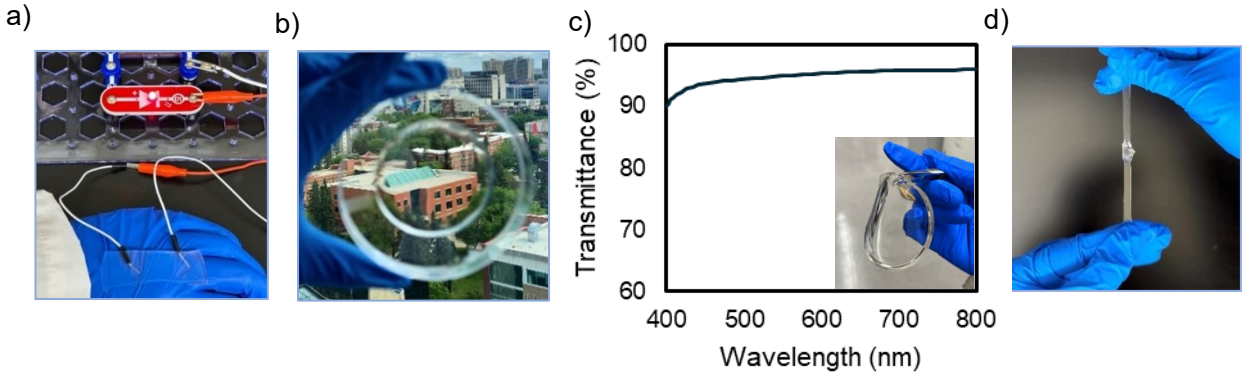

Figure 4.4. (a) Photo showing the conductivity of the composite hydrogel by illuminating a LED lightbulb. (b) Photo showing the optical transparency of the hydrogel, scenery shows clearly through the hydrogel. (c) Optical spectra in the visible light range of the hydrogel at 21˚C. The inset picture shows the appearance of the hydrogel. (d) Photo showing composite hydrogel stretching with a knot.

4.3.4. Strain-sensing performance

The resistance of the hydrogel sensor is highly sensitive to changes in strain, making it suitable for detecting minor strains caused by subtle movements such as touching, tapping, and pressing. Its sensitivity can be quantified by its GF, which varies based on strain rate. Figure 4.3 b shows the relative changes in resistance and GF in response to increasing strain. Figure 4.3 c demonstrates the strain-sensing performance of the hydrogel under cyclic loading and unloading at 100 % and 200 % strain. The as-prepared hydrogel can effectively monitor common gestures that may be used on a soft touch panel such as touching, tapping, and pressing down. In real-life applications, it is critical for the strain sensor to behave consistently (Figure 4.3 d). The hydrogel should show fatigue resistance to mechanical deformation and consistency in relative resistance with repeated cyclic strain given that the sensor is designed for repeated use. In Figure 4.3 e, the relative changes in resistance are shown for 40 cycles of strain at 100 % strain rate. The sensor does not show a visible decrease in sensitivity indicative of damage. Water retention is an important aspect relating to the wearability of a soft sensor.

Regarding the water loss behavior, the interfacial interactions between the hydrogel network and the environment play a pivotal role in dictating the water retention capabilities. The pure PAM hydrogel exhibited a progressive increase in water loss percentage over time, which can be attributed to the gradual evaporation of water molecules under ambient conditions, as well as the weakening of polymer-solvent interactions (Figure 4.5). In contrast, the H-0-0 hydrogel

displayed a slightly reduced rate of water loss, suggesting that the integration of CMC within the hydrogel matrix enhances water retention capabilities. This enhancement can be ascribed to the hydrophilic nature of CMC and the establishment of favorable intermolecular interactions between CMC and PAM, such as hydrogen bonding and van der Waals forces. However, the impacts are not significant.

The H-0.5-0.5 hydrogel saw less than 10 % reduction in mass after four days of exposure to ambient air, while PAM hydrogels and H-0-0 hydrogels saw almost 30 %. After 15 days of exposure to ambient conditions with lid on, the H-0.5-0.5 could still bend, showing signs of flexibility, while the PAM hydrogel becomes completely rigid.

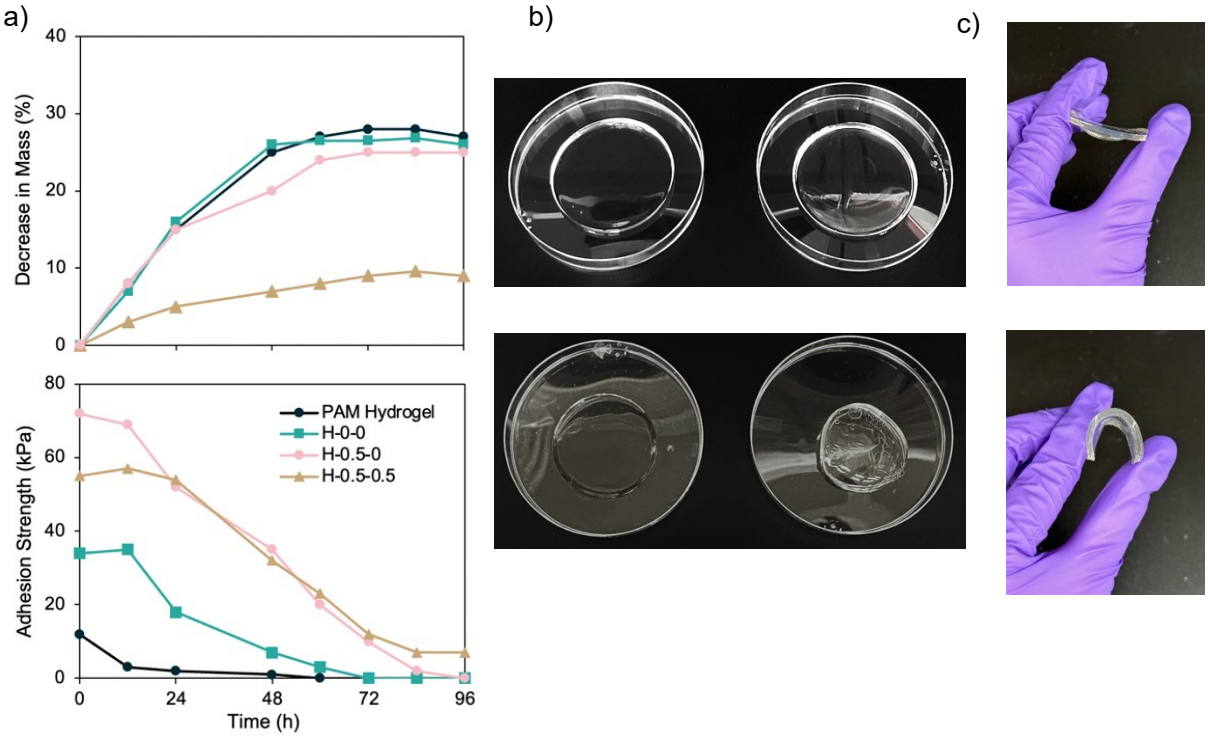

Figure 4.5. (a) Decrease in mass and change in lap-shear adhesion strength of PAM, H-0-0, and H-0.5-0.5 hydrogels over time. (b) H-0.5-0.5 (left) and PAM (right) hydrogel after 15 days. (c) Pictures showing pliability of PAM hydrogel and H-0.5-0.5 after 15 days in ambient condition.

The hydrogel developed in this work demonstrates a remarkable combination of properties compared to other hydrogels based on PAM, polysaccharides and SiW for similar functions found in the literature (Figure 4.6. and Table S2). The strength of the hydrogel reaches 0.54 MPa, a clear indication of the successful balance between adhesive and cohesive forces. Its conductivity of 1.62 S/m is on par with some of the best performing hydrogels in this aspect. Most significantly, the hydrogel exhibits an exceptional strain capacity of 4079% while maintaining an adhesion strength of 80 kPa, significantly outperforming all other hydrogels listed in this comparison. Notably, the PAM/CMC/SiW/LiCl hydrogel is transparent, which is advantageous for applications where optical clarity is essential. By modulating adhesion and cohesion through the addition of silicotungstic acid and adjusting crosslinking density, the PAM/CMC/SiW/LiCl hydrogel exhibits a unique combination of properties, including superior adhesion strength, mechanical robustness, and versatility, setting it apart from other hydrogels reported in the literature and demonstrating its potential for a wide range of applications.

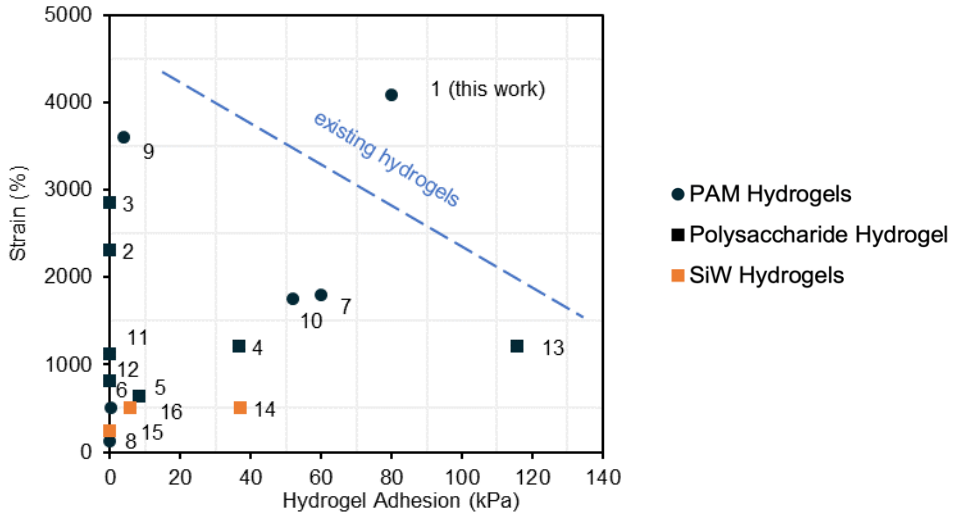

Figure 4.6. Comparison of the performance of this work to similar reported hydrogels.

4.3.5. Rheological Properties and self recovery

Rheological tests were employed to investigate the viscoelastic behavior of the composite hydrogels. Figure 4.7. a shows results from the frequency sweeps of the H-0.5-0.5 hydrogel at a strain of 1% with shear rates ranging from 0.1 to 100 rad/s. The hydrogel displayed a consistently higher storage modulus G′ (elastic behavior) than loss modulus G″ (viscous behavior) regardless of additive concentration, suggesting the dominant elastic property of the hydrogels. Both G′ and G″ showed substantial improvement with an increase in SiW concentration, indicating a higher degree of cross-linking resulting from more intermolecular hydrogen bonds formed between SiW and CMC chains. The composite hydrogel can withstand large shear deformations. In Figure 4.7. b, an oscillatory strain sweeps of H-0.5-0.5 reveals that G′ surpassed the loss modulus G″ up until 300% was applied, where the crossover of the two moduli signified the rupturing of the hydrogel network. Cycling the applied strain between 1% and 1000% (Figure 4.7. d) reveals that dynamic reversible bonds that are ruptured during stretching are quickly and easily reformed without external stimuli, with excellent repeatability. In the temperature sweep (4.7. e), the loss factor of the hydrogel increases less than 0.05 over a range of 20˚C, indicating good thermal stability.

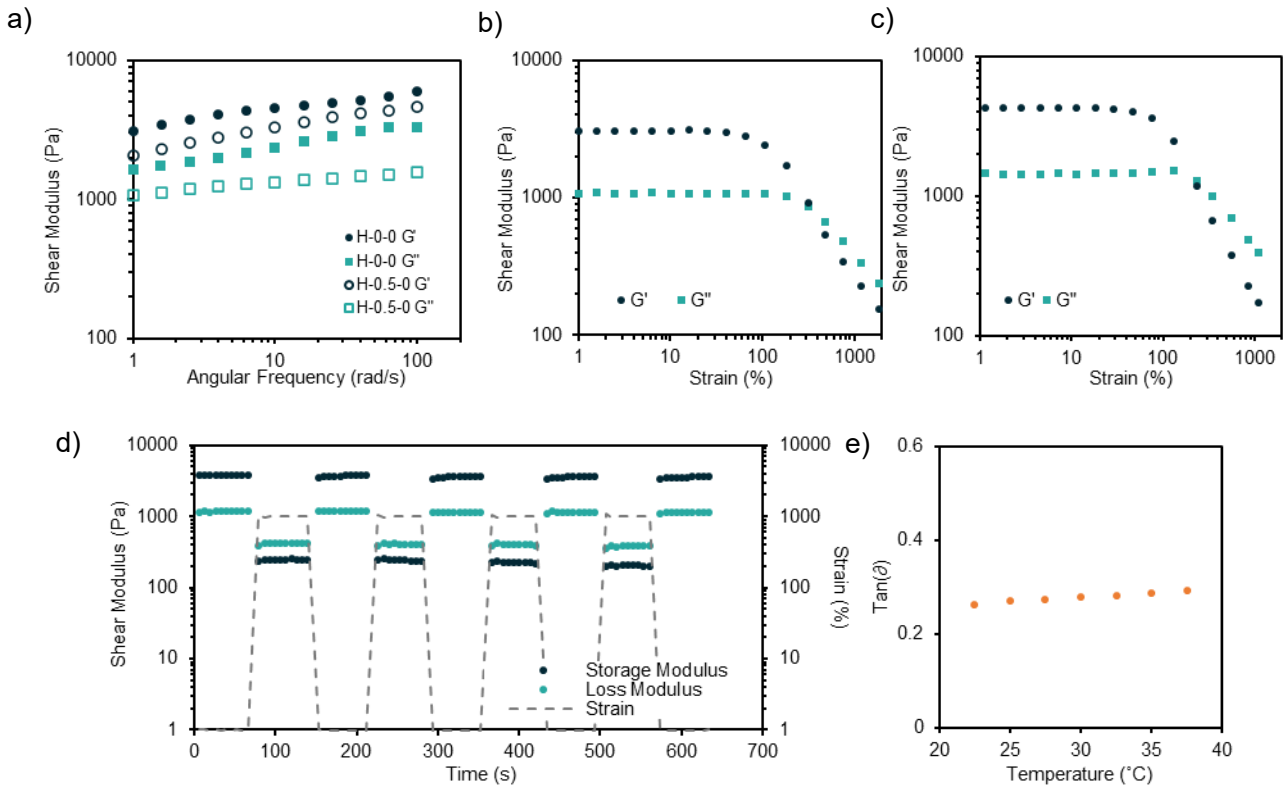

Figure 4.7. (a) Rheological frequency sweep measurements of H-0-0 and H-0.5-0. (b) Rheological oscillatory strain sweeps of H-0.5-0.5 hydrogel. (c) Rheological oscillatory strain sweeps of H-1.0-1.0 hydrogel. (d) Cyclic oscillatory time sweep with the shear strain shifting between 1 % and 1000 % for four cycles. (e) Temperature sweep of H-0.5-0.5 hydrogel.

Silicotungstic acid (SiW) introduces a unique paradigm in the modulation of hydrogel properties due to its ability to establish multifaceted bonding interactions. As a Keggin-type polyoxometalate, SiW possesses a highly symmetrical structure that can enhance crosslinking efficiency in hydrogel networks through both covalent and non-covalent bonds. Covalent crosslinking is critical for establishing the hydrogel's macroscopic mechanical properties, while non-covalent interactions, particularly hydrogen bonds, are reversible and dynamic, allowing for self-healing properties after mechanical damage, which is vital for maintaining long-term structural integrity and functionality in wearable sensor applications.

5. Conclusions and Future Work

In this study, we explore the interplay between cohesion and adhesion in a novel polysaccharide-SiW hydrogel that demonstrates a harmonious balance between mechanical toughness, adhesive capabilities, and biocompatibility, and evaluate its potential and practicality as a wearable strain sensor. This study, therefore, presents an innovative design for a well-rounded and promising material in the field of wearable healthcare technology. This thesis has advanced the field of hydrogel research by focusing on two distinct aspects of SiW-based hydrogels:

(1) PAM/CMC hydrogels with SiW was fabricated and characterized. The hydrogel's synthesis process and its structural properties were studied. The incorporation of SiW into the hydrogel matrix offers a novel and straightforward way for modulation of cohesive and adhesive properties that are seldom investigated in the realm of hydrogel fabrication. The facile modulation of these properties through adjusting the SiW and crosslinker content enables the mechanical properties of the hydrogel to be easily tuned. This study in turn deepens the understanding of how the interplay of cohesive and adhesive forces in a hydrogel can impact its physical performance, thereby enabling the creation of hydrogel with superior mechanical properties while retaining excellent adhesion. Moreover, its ease of fabrication presents a preferable alternative to traditional catechol-based adhesives, providing a practical and versatile material that can be readily integrated into soft and flexible electronics.

(2) The application of PAM/CMC hydrogels with SiW in wearable technology was explored in the second half of this thesis. The as-prepared hydrogel showed adaptability to varying environmental conditions, robustness under mechanical stresses, and its potential

integration into sensor technologies which is rare for high water-content polysaccharide hydrogels that are usually soft and weak. A comprehensive comparison was made between the PAM/CMC hydrogels and previously reported polysaccharide hydrogels of similar applications. The PAM/CMC showed superior mechanical properties, especially stretchability and toughness. The study details how the hydrogel's composition and ionic conductivity make it suitable for various practical applications, such as health monitoring and strain sensing, demonstrating its adaptability to skin surfaces and robustness under diverse conditions. Importantly, this adhesive strength is repeatable and maintains under multi-cyclic testing, demonstrating the hydrogel's resiliency and suitability for repeated use in applications such as wearable strain sensors, aligning with the needs identified for such devices. In addition, the hydrogel demonstrated adhesion to various substrates and stability in water and ambient conditions which many hydrogels lacked. Considering the many advantages, the PAM/CMC hydrogel shows promise in medical applications due to its combination of toughness, adhesiveness, biocompatibility, and reusability, potentially offering enhanced patient monitoring capabilities in wearable medical devices.

The future research directions will focus on:

(1) Biocompatibility: Future studies will specifically focus on the biocompatibility of the polysaccharide-SiW hydrogel. This entails a rigorous assessment of its interaction with living tissue, compatibility with cell lines, and inflammatory response evaluation. In vitro studies will examine the hydrogel's effects on cell viability and proliferation, while in vivo testing will monitor for any adverse immune reactions, ensuring its safety for long-term application in wearable medical devices and potential for implantation.

(2) Industrial-Scale Production and Commercialization: Addressing the challenges of scaling up the production process to meet industrial requirements, especially for wearable technology and healthcare applications.

(3) Advanced Applications and Integration: Expanding the scope of the hydrogel's applications, particularly in the integration with electronic devices for advanced health monitoring systems and exploring its potential in other innovative applications such as drug delivery systems.

Bibliography

(1) Johansson, D.; Malmgren, K.; Alt Murphy, M. Wearable sensors for clinical applications in epilepsy, Parkinson's disease, and stroke: a mixed-methods systematic review. *J Neurol* **2018**, *265* (8), 1740-1752. DOI: 10.1007/s00415-018-8786-y From NLM Medline.

(2) Kim, H.; Kim, K.; Lee, S. J. Nature-inspired thermo-responsive multifunctional membrane adaptively hybridized with PNIPAm and PPy. *NPG Asia Materials* **2017**, *9* (10), e445-e445. DOI: 10.1038/am.2017.168.

(3) Xu, S.; Jayaraman, A.; Rogers, J. A. Skin sensors are the future of health care. *Nature* **2019**, *571* (7765), 319-321.

(4) Vijayalakshmi, K.; Uma, S.; Bhuvanya, R.; Suresh, A. A demand for wearable devices in health care. *Int. J. Eng. Technol* **2018**, *7* (1), 1-4.

(5) Song, J.; Zhang, Y.; Chan, S. Y.; Du, Z.; Yan, Y.; Wang, T.; Li, P.; Huang, W. Hydrogel-based flexible materials for diabetes diagnosis, treatment, and management. *npj Flexible Electronics* **2021**, *5* (1), 26.

(6) Sun, J.-Y.; Zhao, X.; Illeperuma, W. R.; Chaudhuri, O.; Oh, K. H.; Mooney, D. J.; Vlassak, J. J.; Suo, Z. Highly stretchable and tough hydrogels. *Nature* **2012**, *489* (7414), 133-136.

(7) Seshadri, D. R.; Li, R. T.; Voos, J. E.; Rowbottom, J. R.; Alfes, C. M.; Zorman, C. A.; Drummond, C. K. Wearable sensors for monitoring the internal and external workload of the athlete. *NPJ digital medicine* **2019**, *2* (1), 71.

(8) Hou, C.; Wang, H.; Zhang, Q.; Li, Y.; Zhu, M. Highly conductive, flexible, and compressible all-graphene passive electronic skin for sensing human touch. *Advanced Materials* **2014**, *26* (29), 5018-5024.

(9) Peng, Q.; Chen, J.; Zeng, Z.; Wang, T.; Xiang, L.; Peng, X.; Liu, J.; Zeng, H. Adhesive Coacervates Driven by Hydrogen-Bonding Interaction. *Small* **2020**, *16* (43), 2004132.

(10) Chen, J.; Liu, J.; Thundat, T.; Zeng, H. Polypyrrole-doped conductive supramolecular elastomer with stretchability, rapid self-healing, and adhesive property for flexible electronic sensors. *ACS applied materials & interfaces* **2019**, *11* (20), 18720-18729.

(11) Gan, D.; Huang, Z.; Wang, X.; Jiang, L.; Wang, C.; Zhu, M.; Ren, F.; Fang, L.; Wang, K.; Xie, C. Graphene oxide-templated conductive and redox-active nanosheets incorporated hydrogels for adhesive bioelectronics. *Advanced Functional Materials* **2020**, *30* (5), 1907678.

(12) Kristoffersson, A.; Lindén, M. A systematic review of wearable sensors for monitoring physical activity. *Sensors* **2022**, *22* (2), 573.

(13) Regterschot, G. R. H.; Ribbers, G. M.; Bussmann, J. B. Wearable movement sensors for rehabilitation: From technology to clinical practice. MDPI: 2021; Vol. 21, p 4744.

(14) Brognara, L.; Palumbo, P.; Grimm, B.; Palmerini, L. Assessing gait in Parkinson's disease using wearable motion sensors: a systematic review. *Diseases* **2019**, *7* (1), 18.

(15) Porciuncula, F.; Roto, A. V.; Kumar, D.; Davis, I.; Roy, S.; Walsh, C. J.; Awad, L. N. Wearable movement sensors for rehabilitation: a focused review of technological and clinical advances. *Pm&r* **2018**, *10* (9), S220-S232.

(16) Wu, M.; Chen, J.; Ma, Y.; Yan, B.; Pan, M.; Peng, Q.; Wang, W.; Han, L.; Liu, J.; Zeng, H. Ultra elastic, stretchable, self-healing conductive hydrogels with tunable optical properties for highly sensitive soft electronic sensors. *Journal of Materials Chemistry A* **2020**, *8* (46), 24718-24733.

(17) Wichterle, O.; Lim, D. Hydrophilic gels for biological use. *Nature* **1960**, *185* (4706), 117-118.

(18) Zhao, Y.; Lu, W.; Shen, S.; Wei, L. Chitosan derivative-based mussel-inspired hydrogels as the dressings and drug delivery systems in wound healing. *Cellulose* **2021**, *28*, 11429-11450.

(19) Abasalizadeh, F.; Moghaddam, S. V.; Alizadeh, E.; Akbari, E.; Kashani, E.; Fazljou, S. M. B.; Torbati, M.; Akbarzadeh, A. Alginate-based hydrogels as drug delivery vehicles in cancer treatment and their applications in wound dressing and 3D bioprinting. *Journal of biological engineering* **2020**, *14*, 1-22.

(20) Xinming, L.; Yingde, C.; Lloyd, A. W.; Mikhalovsky, S. V.; Sandeman, S. R.; Howel, C. A.; Liewen, L. Polymeric hydrogels for novel contact lens-based ophthalmic drug delivery systems: A review. *Contact Lens and Anterior Eye* **2008**, *31* (2), 57-64.

(21) Pimenta, A.; Ascenso, J.; Fernandes, J.; Colaço, R.; Serro, A.; Saramago, B. Controlled drug release from hydrogels for contact lenses: Drug partitioning and diffusion. *International journal of pharmaceutics* **2016**, *515* (1-2), 467-475.

(22) Paradiso, P.; Serro, A. P.; Saramago, B.; Colaço, R.; Chauhan, A. Controlled release of antibiotics from vitamin E–loaded silicone-hydrogel contact lenses. *Journal of Pharmaceutical Sciences* **2016**, *105* (3), 1164-1172.

(23) Maulvi, F. A.; Lakdawala, D. H.; Shaikh, A. A.; Desai, A. R.; Choksi, H. H.; Vaidya, R. J.; Ranch, K. M.; Koli, A. R.; Vyas, B. A.; Shah, D. O. In vitro and in vivo evaluation of novel implantation technology in hydrogel contact lenses for controlled drug delivery. *Journal of Controlled Release* **2016**, *226*, 47-56.

(24) Puvirajesinghe, T. M.; Zhi, Z.; Craster, R. V.; Guenneau, S. Tailoring drug release rates in hydrogel-based therapeutic delivery applications using graphene oxide. *Journal of the Royal Society Interface* **2018**, *15* (139), 20170949.

(25) Hu, Y.; Hu, S.; Zhang, S.; Dong, S.; Hu, J.; Kang, L.; Yang, X. A double-layer hydrogel based on alginate-carboxymethyl cellulose and synthetic polymer as sustained drug delivery system. *Scientific reports* **2021**, *11* (1), 9142.

(26) Lee, S. C.; Kwon, I. K.; Park, K. Hydrogels for delivery of bioactive agents: A historical perspective. *Advanced drug delivery reviews* **2013**, *65* (1), 17-20.

(27) Hoffman, A. S. Hydrogels for biomedical applications. *Advanced drug delivery reviews* **2012**, *64*, 18-23.

(28) Lin, C.-C.; Metters, A. T. Hydrogels in controlled release formulations: network design and mathematical modeling. *Advanced drug delivery reviews* **2006**, *58* (12-13), 1379-1408.

(29) Hoare, T. R.; Kohane, D. S. Hydrogels in drug delivery: Progress and challenges. *polymer* **2008**, *49* (8), 1993-2007.

(30) Ashley, G. W.; Henise, J.; Reid, R.; Santi, D. V. Hydrogel drug delivery system with predictable and tunable drug release and degradation rates. *Proceedings of the national academy of sciences* **2013**, *110* (6), 2318-2323.

(31) Hwang, C.-W.; Wu, D.; Edelman, E. R. Physiological transport forces govern drug distribution for stent-based delivery. *Circulation* **2001**, *104* (5), 600-605.

(32) Li, J.; Mooney, D. J. Designing hydrogels for controlled drug delivery. *Nature Reviews Materials* **2016**, *1* (12), 1-17.

(33) Siepmann, J.; Göpferich, A. Mathematical modeling of bioerodible, polymeric drug delivery systems. *Advanced drug delivery reviews* **2001**, *48* (2-3), 229-247.

(34) Sun, Z.; Song, C.; Wang, C.; Hu, Y.; Wu, J. Hydrogel-based controlled drug delivery for cancer treatment: a review. *Molecular pharmaceutics* **2019**, *17* (2), 373-391.

(35) Hamidi, M.; Azadi, A.; Rafiei, P. Hydrogel nanoparticles in drug delivery. *Advanced drug delivery reviews* **2008**, *60* (15), 1638-1649.

(36) Hu, X.; Gong, X. A new route to fabricate biocompatible hydrogels with controlled drug delivery behavior. *Journal of colloid and interface science* **2016**, *470*, 62-70.

(37) Weiser, J. R.; Saltzman, W. M. Controlled release for local delivery of drugs: barriers and models. *Journal of Controlled Release* **2014**, *190*, 664-673.

(38) Huang, X.; Ge, G.; She, M.; Ma, Q.; Lu, Y.; Zhao, W.; Shen, Q.; Wang, Q.; Shao, J. Self-healing hydrogel with multiple dynamic interactions for multifunctional epidermal sensor. *Applied Surface Science* **2022**, *598*, 153803.

(39) Sun, X.; Agate, S.; Salem, K. S.; Lucia, L.; Pal, L. Hydrogel-based sensor networks: Compositions, properties, and applications—A review. *ACS Applied Bio Materials* **2020**, *4* (1), 140-162.

(40) Buenger, D.; Topuz, F.; Groll, J. Hydrogels in sensing applications. *Progress in Polymer Science* **2012**, *37* (12), 1678-1719.

(41) Tai, Y.; Mulle, M.; Ventura, I. A.; Lubineau, G. A highly sensitive, low-cost, wearable pressure sensor based on conductive hydrogel spheres. *Nanoscale* **2015**, *7* (35), 14766-14773.

(42) Pan, L.; Han, L.; Liu, H.; Zhao, J.; Dong, Y.; Wang, X. Flexible sensor based on Hair-like microstructured ionic hydrogel with high sensitivity for pulse wave detection. *Chemical Engineering Journal* **2022**, *450*, 137929.

(43) Wu, M.; Pan, M.; Qiao, C.; Ma, Y.; Yan, B.; Yang, W.; Peng, Q.; Han, L.; Zeng, H. Ultra stretchable, tough, elastic and transparent hydrogel skins integrated with intelligent sensing functions enabled by machine learning algorithms. *Chemical Engineering Journal* **2022**, *450*, 138212.

(44) Peng, X.; Wang, W.; Yang, W.; Chen, J.; Peng, Q.; Wang, T.; Yang, D.; Wang, J.; Zhang, H.; Zeng, H. Stretchable, compressible, and conductive hydrogel for sensitive wearable soft sensors. *Journal of Colloid and Interface Science* **2022**, *618*, 111-120.

(45) Xia, S.; Zhang, Q.; Song, S.; Duan, L.; Gao, G. Bioinspired dynamic cross-linking hydrogel sensors with skin-like strain and pressure sensing behaviors. *Chemistry of Materials* **2019**, *31* (22), 9522-9531.

(46) Xia, S.; Song, S.; Jia, F.; Gao, G. A flexible, adhesive and self-healable hydrogel-based wearable strain sensor for human motion and physiological signal monitoring. *Journal of Materials Chemistry B* **2019**, *7* (30), 4638-4648.

(47) Liao, M.; Wan, P.; Wen, J.; Gong, M.; Wu, X.; Wang, Y.; Shi, R.; Zhang, L. Wearable, healable, and adhesive epidermal sensors assembled from mussel-inspired conductive hybrid hydrogel framework. *Advanced Functional Materials* **2017**, *27* (48), 1703852.

(48) Wang, Z.; Chen, J.; Cong, Y.; Zhang, H.; Xu, T.; Nie, L.; Fu, J. Ultrastretchable strain sensors and arrays with high sensitivity and linearity based on super tough conductive hydrogels. *Chemistry of Materials* **2018**, *30* (21), 8062-8069.

(49) Sun, F.; Huang, X.; Wang, X.; Liu, H.; Wu, Y.; Du, F.; Zhang, Y. Highly transparent, adhesive, stretchable and conductive PEDOT: PSS/polyacrylamide hydrogels for flexible strain sensors. *Colloids and Surfaces A: Physicochemical and Engineering Aspects* **2021**, *625*, 126897.

(50) Han, S.; Liu, C.; Lin, X.; Zheng, J.; Wu, J.; Liu, C. Dual conductive network hydrogel for a highly conductive, self-healing, anti-freezing, and non-drying strain sensor. *ACS Applied Polymer Materials* **2020**, *2* (2), 996-1005.

(51) Feng, Y.; Liu, H.; Zhu, W.; Guan, L.; Yang, X.; Zvyagin, A. V.; Zhao, Y.; Shen, C.; Yang, B.; Lin, Q. Muscle-inspired MXene conductive hydrogels with anisotropy and low-temperature

tolerance for wearable flexible sensors and arrays. *Advanced Functional Materials* **2021**, *31* (46), 2105264.

(52) Liao, H.; Guo, X.; Wan, P.; Yu, G. Conductive MXene nanocomposite organohydrogel for flexible, healable, low-temperature tolerant strain sensors. *Advanced Functional Materials* **2019**, *29* (39), 1904507.

(53) Huang, T.; Xu, H.; Jiao, K.; Zhu, L.; Brown, H. R.; Wang, H. A novel hydrogel with high mechanical strength: a macromolecular microsphere composite hydrogel. *Advanced Materials* **2007**, *19* (12), 1622-1626.

(54) Ding, H.; Liang, X.; Wang, Q.; Wang, M.; Li, Z.; Sun, G. A semi-interpenetrating network ionic composite hydrogel with low modulus, fast self-recoverability and high conductivity as flexible sensor. *Carbohydrate Polymers* **2020**, *248*, 116797.

(55) Yi, J.; Nguyen, K.-C. T.; Wang, W.; Yang, W.; Pan, M.; Lou, E.; Major, P. W.; Le, L. H.; Zeng, H. Mussel-inspired adhesive double-network hydrogel for intraoral ultrasound imaging. *ACS Applied Bio Materials* **2020**, *3* (12), 8943-8952.

(56) Wang, S.; Cheng, H.; Yao, B.; He, H.; Zhang, L.; Yue, S.; Wang, Z.; Ouyang, J. Self-adhesive, stretchable, biocompatible, and conductive nonvolatile eutectogels as wearable conformal strain and pressure sensors and biopotential electrodes for precise health monitoring. *ACS Applied Materials & Interfaces* **2021**, *13* (17), 20735-20745.

(57) Zafar, S.; Hanif, M.; Azeem, M.; Mahmood, K.; Gondal, S. A. Role of crosslinkers for synthesizing biocompatible, biodegradable and mechanically strong hydrogels with desired release profile. *Polymer Bulletin* **2021**, 1-21.

(58) Li, Q.; Wang, L.; Liu, Q.; Hong, W.; Yang, C. Fatigue Damage–Resistant Physical Hydrogel Adhesion. *Frontiers in Robotics and AI* **2021**, *8*, 666343.

(59) Zhang, T.; Yuk, H.; Lin, S.; Parada, G. A.; Zhao, X. Tough and tunable adhesion of hydrogels: experiments and models. *Acta Mechanica Sinica* **2017**, *33*, 543-554.

(60) Liu, J.; Lin, S.; Liu, X.; Qin, Z.; Yang, Y.; Zang, J.; Zhao, X. Fatigue-resistant adhesion of hydrogels. *Nature communications* **2020**, *11* (1), 1071.

(61) Zhang, M.; Zhang, D.; Chen, H.; Zhang, Y.; Liu, Y.; Ren, B.; Zheng, J. A multiscale polymerization framework towards network structure and fracture of double-network hydrogels. *npj Computational Materials* **2021**, *7* (1), 39.

(62) Mirkhalaf, M.; Yazdani Sarvestani, H.; Yang, Q.; Jakubinek, M. B.; Ashrafi, B. A comparative study of nano-fillers to improve toughness and modulus of polymer-derived ceramics. *Scientific reports* **2021**, *11* (1), 6951.

(63) Zaragoza, J.; Fukuoka, S.; Kraus, M.; Thomin, J.; Asuri, P. Exploring the role of nanoparticles in enhancing mechanical properties of hydrogel nanocomposites. *Nanomaterials* **2018**, *8* (11), 882.

(64) Xue, B.; Gu, J.; Li, L.; Yu, W.; Yin, S.; Qin, M.; Jiang, Q.; Wang, W.; Cao, Y. Hydrogel tapes for fault-tolerant strong wet adhesion. *Nature Communications* **2021**, *12* (1), 7156.

(65) Haque, M. A.; Kurokawa, T.; Gong, J. P. Super tough double network hydrogels and their application as biomaterials. *Polymer* **2012**, *53* (9), 1805-1822.

(66) Rebers, L.; Reichsöllner, R.; Regett, S.; Tovar, G. E.; Borchers, K.; Baudis, S.; Southan, A. Differentiation of physical and chemical cross-linking in gelatin methacryloyl hydrogels. *Scientific reports* **2021**, *11* (1), 3256.

(67) Uchida, M.; Sengoku, T.; Kaneko, Y.; Okumura, D.; Tanaka, H.; Ida, S. Evaluation of the effects of cross-linking and swelling on the mechanical behaviors of hydrogels using the digital image correlation method. *Soft Matter* **2019**, *15* (16), 3389-3396.

(68) Siddiqua, A.; Ranjha, N. M.; Rehman, S.; Shoukat, H.; Ramzan, N.; Sultana, H. Preparation and characterization of methylene bisacrylamide crosslinked pectin/acrylamide hydrogels. *Polymer Bulletin* **2022**, *79* (9), 7655-7677.

(69) Risbud, M. V.; Bhonde, R. R. Polyacrylamide-chitosan hydrogels: in vitro biocompatibility and sustained antibiotic release studies. *Drug Delivery* **2000**, *7* (2), 69-75.

(70) Shariatinia, Z.; Jalali, A. M. Chitosan-based hydrogels: Preparation, properties and applications. *International journal of biological macromolecules* **2018**, *115*, 194-220.

(71) Jin, X.; Jiang, H.; Zhang, Z.; Yao, Y.; Bao, X.; Hu, Q. Ultrastretchable, self-adhesive, strain-sensitive and self-healing GO@ DA/Alginate/P (AAc-co-AAm) multifunctional hydrogels via mussel-inspired chemistry. *Carbohydrate Polymers* **2021**, *254*, 117316.

(72) Aarstad, O.; Heggset, E. B.; Pedersen, I. S.; Bjørnøy, S. H.; Syverud, K.; Strand, B. L. Mechanical properties of composite hydrogels of alginate and cellulose nanofibrils. *Polymers* **2017**, *9* (8), 378.

(73) Wang, C.; Bai, J.; Tian, P.; Xie, R.; Duan, Z.; Lv, Q.; Tao, Y. The application status of nanoscale cellulose-based hydrogels in tissue engineering and regenerative biomedicine. *Frontiers in Bioengineering and Biotechnology* **2021**, *9*, 732513.

(74) El Fawal, G. F.; Abu-Serie, M. M.; Hassan, M. A.; Elnouby, M. S. Hydroxyethyl cellulose hydrogel for wound dressing: Fabrication, characterization and in vitro evaluation. *International journal of biological macromolecules* **2018**, *111*, 649-659.

(75) Jeong, D.; Joo, S.-W.; Hu, Y.; Shinde, V. V.; Cho, E.; Jung, S. Carboxymethyl cellulose-based superabsorbent hydrogels containing carboxymehtyl β-cyclodextrin for enhanced mechanical strength and effective drug delivery. *European Polymer Journal* **2018**, *105*, 17-25.

(76) Rahman, M. A.; Bowland, C.; Ge, S.; Acharya, S. R.; Kim, S.; Cooper, V. R.; Chen, X. C.; Irle, S.; Sokolov, A. P.; Savara, A. Design of tough adhesive from commodity thermoplastics through dynamic crosslinking. *Science advances* **2021**, *7* (42), eabk2451.

(77) Aswathy, S. H.; NarendraKumar, U.; Manjubala, I. Physicochemical properties of cellulose-based hydrogel for biomedical applications. *Polymers* **2022**, *14* (21), 4669.

(78) Hsu, W.-H.; Kao, Y.-C.; Chuang, S.-H.; Wang, J.-S.; Lai, J.-Y.; Tsai, H.-C. Thermosensitive double network of zwitterionic polymers for controlled mechanical strength of hydrogels. *RSC advances* **2019**, *9* (42), 24241-24247.

(79) Nkhwa, S.; Kemal, E.; Gurav, N.; Deb, S. Dual polymer networks: a new strategy in expanding the repertoire of hydrogels for biomedical applications. *Journal of Materials Science: Materials in Medicine* **2019**, *30*, 1-14.

(80) Xie, S.; Chen, Y.; Guo, Z.; Luo, Y.; Tan, H.; Xu, L.; Xu, J.; Zheng, J. Agar/carbon dot crosslinked polyacrylamide double-network hydrogels with robustness, self-healing, and stimulus-response fluorescence for smart anti-counterfeiting. *Materials Chemistry Frontiers* **2021**, *5* (14), 5418-5428.

(81) Yu, Z.; Zhang, Y.; Gao, Z. J.; Ren, X. Y.; Gao, G. H. Enhancing mechanical strength of hydrogels via IPN structure. *Journal of Applied Polymer Science* **2017**, *134* (8).

(82) Liu, L.; Chen, Y.; Zhao, C.; Guo, M.; Wu, Y.; Li, Y.; Xiang, D.; Li, H.; Wang, L.; Zhang, X. Highly sensitive, super high stretchable hydrogel strain sensor with underwater repeated adhesion and rapid healing. *Polymer* **2023**, *285*, 126317.

(83) Zhang, W.; Zhang, Y.; Zhang, Y.; Dai, Y.; Xia, F.; Zhang, X. Adhesive and tough hydrogels: from structural design to applications. *Journal of Materials Chemistry B* **2021**, *9* (30), 5954-5966.

(84) Wu, L.; Li, L.; Qu, M.; Wang, H.; Bin, Y. Mussel-inspired self-adhesive, antidrying, and antifreezing poly (acrylic acid)/bentonite/polydopamine hybrid glycerol-hydrogel and the sensing application. *ACS Applied Polymer Materials* **2020**, *2* (8), 3094-3106.

(85) Fan, H.; Gong, J. P. Bioinspired underwater adhesives. *Advanced Materials* **2021**, *33* (44), 2102983.

(86) Zhu, X.; Wei, C.; Chen, H.; Zhang, C.; Peng, H.; Wang, D.; Yuan, J.; Waite, J. H.; Zhao, Q. A Cation-Methylene-Phenyl sequence encodes programmable poly (ionic liquid) coacervation and robust underwater adhesion. *Advanced Functional Materials* **2022**, *32* (2), 2105464.

(87) Jing, B.; Wang, X.; Wang, H.; Qiu, J.; Shi, Y.; Gao, H.; Zhu, Y. Shape and mechanical control of poly (ethylene oxide) based polymersome with polyoxometalates via hydrogen bond. *The Journal of Physical Chemistry B* **2017**, *121* (7), 1723-1730.

(88) Dolbecq, A.; Dumas, E.; Mayer, C. R.; Mialane, P. Hybrid organic− inorganic polyoxometalate compounds: from structural diversity to applications. *Chemical reviews* **2010**, *110* (10), 6009-6048.

(89) Xu, J.; Li, X.; Li, J.; Li, X.; Li, B.; Wang, Y.; Wu, L.; Li, W. Wet and functional adhesives from one-step aqueous self-assembly of natural amino acids and polyoxometalates. *Angewandte Chemie* **2017**, *129* (30), 8857-8861.

(90) Liu, C.; Zhang, R.; Li, P.; Qu, J.; Chao, P.; Mo, Z.; Yang, T.; Qing, N.; Tang, L. Conductive hydrogels with ultrastretchability and adhesiveness for flame-and cold-tolerant strain sensors. *ACS Applied Materials & Interfaces* **2022**, *14* (22), 26088-26098.

(91) Shin, S. R.; Jung, S. M.; Zalabany, M.; Kim, K.; Zorlutuna, P.; Kim, S. b.; Nikkhah, M.; Khabiry, M.; Azize, M.; Kong, J. Carbon-nanotube-embedded hydrogel sheets for engineering cardiac constructs and bioactuators. *ACS nano* **2013**, *7* (3), 2369-2380.

(92) Vashist, A.; Kaushik, A.; Vashist, A.; Sagar, V.; Ghosal, A.; Gupta, Y.; Ahmad, S.; Nair, M. Advances in carbon nanotubes–hydrogel hybrids in nanomedicine for therapeutics. *Advanced Healthcare Materials* **2018**, *7* (9), 1701213.

(93) Mir, A.; Kumar, A.; Riaz, U. A short review on the synthesis and advance applications of polyaniline hydrogels. *RSC advances* **2022**, *12* (30), 19122-19132.

(94) Pyarasani, R. D.; Jayaramudu, T.; John, A. Polyaniline-based conducting hydrogels. *Journal of Materials Science* **2019**, *54* (2), 974-996.

(95) Ren, J.; Zhang, A.; Zhang, L.; Li, Y.; Yang, W. Electrically conductive and mechanically tough graphene nanocomposite hydrogels with self - oscillating performance. *Polymer International* **2019**, *68* (6), 1146-1154.

(96) Jo, H.; Sim, M.; Kim, S.; Yang, S.; Yoo, Y.; Park, J.-H.; Yoon, T. H.; Kim, M.-G.; Lee, J. Y. Electrically conductive graphene/polyacrylamide hydrogels produced by mild chemical reduction for enhanced myoblast growth and differentiation. *Acta Biomaterialia* **2017**, *48*, 100-109.

(97) Kim, C.-C.; Lee, H.-H.; Oh, K. H.; Sun, J.-Y. Highly stretchable, transparent ionic touch panel. *Science* **2016**, *353* (6300), 682-687.

(98) Lei, Z.; Wang, Q.; Sun, S.; Zhu, W.; Wu, P. A bioinspired mineral hydrogel as a self-healable, mechanically adaptable ionic skin for highly sensitive pressure sensing. *Advanced Materials* **2017**, *29* (22), 1700321.

(99) Hartshorn, S. R. *Structural adhesives: chemistry and technology*; Springer Science & Business Media, 2012.

(100) Xu, J.; Li, X.; Li, X.; Li, B.; Wu, L.; Li, W.; Xie, X.; Xue, R. Supramolecular copolymerization of short peptides and polyoxometalates: toward the fabrication of underwater adhesives. *Biomacromolecules* **2017**, *18* (11), 3524-3530.

(101) Corpart, J. M.; Candau, F. Aqueous solution properties of ampholytic copolymers prepared in microemulsions. *Macromolecules* **1993**, *26* (6), 1333-1343.

(102) Loeffler, H. H.; Rode, B. M. The hydration structure of the lithium ion. *The Journal of chemical physics* **2002**, *117* (1), 110-117.

(103) Gubitosi, M.; Duarte, H.; Gentile, L.; Olsson, U.; Medronho, B. On cellulose dissolution and aggregation in aqueous tetrabutylammonium hydroxide. *Biomacromolecules* **2016**, *17* (9), 2873-2881.

(104) Gao, C.; Liu, M.; Chen, J.; Zhang, X. Preparation and controlled degradation of oxidized sodium alginate hydrogel. *Polymer degradation and stability* **2009**, *94* (9), 1405-1410.

(105) Mazzotta, M. G.; Putnam, A. A.; North, M. A.; Wilker, J. J. Weak bonds in a biomimetic adhesive enhance toughness and performance. *Journal of the American Chemical Society* **2020**, *142* (10), 4762-4768.

(106) Heinzmann, C.; Weder, C.; de Espinosa, L. M. Supramolecular polymer adhesives: advanced materials inspired by nature. *Chemical Society Reviews* **2016**, *45* (2), 342-358.

(107) Adams, R. D. *Adhesive bonding: science, technology and applications*; Woodhead Publishing, 2021.

(108) Meredith, H. J.; Wilker, J. J. The interplay of modulus, strength, and ductility in adhesive design using biomimetic polymer chemistry. *Advanced Functional Materials* **2015**, *25* (31), 5057-5065.

(109) Lin, W.; Klein, J. Hydration lubrication in biomedical applications: From cartilage to hydrogels. *Accounts of materials research* **2022**, *3* (2), 213-223.

Appendix

1. Details for hydrogel compositions and performance

Table S1. The Compositions of the PAM/CMC Hydrogels

Hydrogels	AM (g)	CMC (g)	SiW (wt%)	LiCl (wt%)	MBAA (wt%)
H-0-0	2	0.6	0	0	0.012
H-0.25-0	2	0.6	0.25	0	0.012
H-0.5-0	2	0.6	0.5	0	0.012
H-0.75-0	2	0.6	0.75	0	0.012
H-1.0-0	2	0.6	1.0	0	0.012
H-0.5-0.25	2	0.6	0.5	0.25	0.012
H-0.5-0.5	2	0.6	0.5	0.5	0.012
H-0.5-0.5l	2	0.6	0.5	0.5	0.012 (low)
H-0.5-0.5r	2	0.6	0.5	0.5	0.018 (medium)
H-0.5-0.5h	2	0.6	0.5	0.5	0.024 (high)-

Table S2. Comparison of PAM/CMC hydrogel to similar hydrogels in literature

Study No.	Composition	Hydrogel Adhesion (kPa)	Hydrogel Strength (MPa)	Conductivity (S/m)	Strain (%)	Transparency
1	PAM/CMC/SiW/LiCl (This work)	80	0.54	1.62	4079	transparent
2	PAM/Alginate	-	0.16	-	2300	transparent
3	P(AMPS/AAm)/CS	-	0.81	1.82	2839	translucent
4	Alginate/P(AAc-co-AAm)/GO@DA	36.9	0.32	3.24	1198	translucent
5	P(AAm-co-VI)/QCS-Fe3+	8.4	0.25	3.83	633	opaque
6	PAMPS	0.12	0.09	-	509	transparent
7	TA/PVA/PAM/VKCl	60	0.32	4	1800	transparent
8	PEDOT:PSS-P(AAM-co-MAA)	-	0.07	0.06	129	translucent
9	PAM/CNF/TA	4	0.2	0.56	3600	translucent
10	PAM/SS/NaCl	52	0,36	1.68	1750	transparent
11	CMC/PAM/Fe3+	-	1.85	1.82	1115	translucent
12	CMC/PAM/NaCl	-	0.43	6.44	800	translucent
13	DES/CNCs/PVA/CMC-Na	116	0.9	0.04	1200	transparent
14	HPMC/SiW-PDMAEMA/Fe3+	37	-	-	500	opaque
15	PAM/CH/SiW	0			234	
16	CS/SiW-PAM	6	-		500	

Figure S.1. Photograph of as-prepared H-0.5-0.5 hydrogel showing high transparency

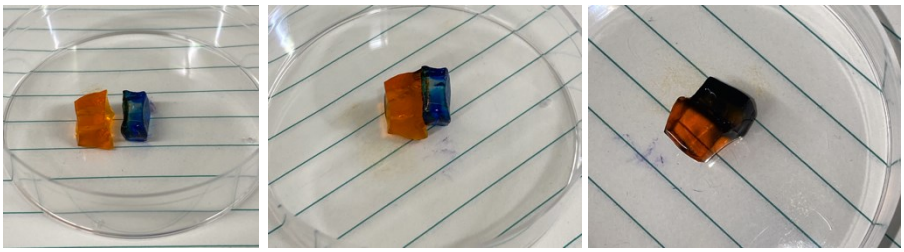

Figure S.2. Self-healing of H-0.5-0.5 hydrogel

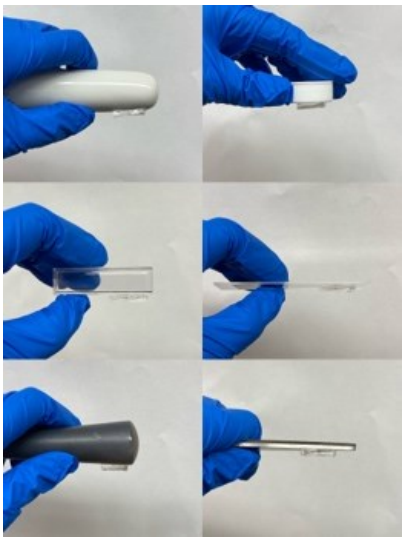

Figure S.3. H-0.5-0.5 adhesion to a variety of substrates, including porcelain, polypropylene, poly(methyl methacrylate), glass, agate, stainless steel.